Ukrainian Journal of Physical Optics
ISSUE 4
2026

STOCHASTIC (3+1)-DIMENSIONAL SPATIO-TEMPORAL SOLITONS IN A GENERALIZED EFFECTIVE FIBER BRAGG-GRATING ENVELOPE MODEL

AHMED S. M. METWALLY [1], MOHAMED E. M. ALNGAR [2], REHAM M. A. SHOHIB [3], SAGAR E. SHIRSATH [4], ANJAN BISWAS [5,6,7,8,9*]

[1] Center of Excellence for Research in Science and Mathematics Education Development, DSR, King Saud University, P.O. Box 11451, Riyadh, Saudi Arabia
[2] Mathematics Education Program, Faculty of Education and Arts, Sohar University, Sohar 311, Oman
[3] Basic Science Department, Faculty of Economics and Business Administration, Innovation University, Sharqia, Egypt
[4] School of Materials Science and Engineering, University of New South Wales, Sydney, NSW, 2052, Australia
[5] Department of Mathematics & Physics, Grambling State University, Grambling, LA 71245—2715, USA
[6] Department of Mathematics, Faculty of Science, Karadeniz Technical University, Trabzon—61080, Türkiye
[7] Department of Physics and Electronics, Khazar University, Baku, AZ—1096, Azerbaijan
[8] Applied Science Research Center, Applied Science Private University, Amman—11937, Jordan
[9] Department of Mathematics and Applied Mathematics, Sefako Makgatho Health Sciences University, Medunsa–0204, Pretoria, South Africa
*Corresponding author: biswas.anjan@gmail.com

Received: 08.08.2026

Abstract. This paper investigates a (3+1)-dimensional stochastic coupled nonlinear Schrödinger (NLS) system interpreted as a generalized effective envelope model for Fiber Bragg grating (FBG) media. The mathematical structure of the coupled stochastic framework was originally introduced for birefringent optical fibers, while this study extends it to the FBG setting to describe interacting optical field components under the combined influence of chromatic and spatiotemporal dispersion, self- and cross-phase modulation, intermodal coupling, four-wave mixing, and multiplicative white-noise perturbations. By applying the modified Sub-ODE method, we obtain several exact analytical solution families, including bright, dark, and singular solitons, periodic waveforms, and solutions expressed in terms of Jacobi elliptic and Weierstrass functions. The corresponding parameter and admissibility conditions are derived explicitly, providing a unified analytical description of the resulting stochastic nonlinear wave structures. Representative solutions illustrate the influence of the stochastic parameter on the phase characteristics and wave profiles within the adopted effective FBG framework. These results extend the analytical treatment of stochastic higher-dimensional coupled-wave systems and provide further insight into nonlinear, dispersive, and noise-driven dynamics in generalized grating-fiber media.

Keywords: stochastic nonlinear Schrödinger equation, fiber Bragg grating, bright and dark solitons, elliptic function solutions, noise-driven dynamics
UDC: 535.18
DOI: 10.3116/16091833/Ukr.J.Phys.Opt.2026.04102

1. Introduction

The nonlinear Schrödinger (NLS) equation is a cornerstone model for coherent wave dynamics in dispersive, nonlinear media, with influential applications to fiber Bragg gratings (FBGs), where periodic index modulation enables dispersion engineering and Bragg solitons [1]. In FBGs, diverse nonlinear responses, including Kerr, quadratic-cubic, and polynomial laws, have been shown to sustain a rich set of waveforms and management strategies relevant to modern photonics [2–5].

Realistic photonic platforms are not purely deterministic: thermal fluctuations, spontaneous emission, and environmental perturbations inject randomness that reshapes coherence, stability, and transport. This has motivated stochastic extensions of NLS-type models, where multiplicative noise can alter soliton amplitudes, velocities, and lifetimes and induce noise-mediated transitions [6]. Recent studies have developed stochastic formulations for FBG and related media, including Itô driving and additional physical effects such as differential group delay [7–9].

Concurrently, stochastic Fokas–Lenells (FL) models tailored to FBGs and birefringent fibers have emerged, yielding explicit noise-driven waveforms and soliton families that bridge deterministic theory with randomness-aware analysis [10–13]. On the deterministic side, the FL hierarchy refines NLS to capture nonparaxial and spatio-temporal effects and admits a mature toolbox, including perturbation theory, inverse-scattering frameworks, global well-posedness, and high-order solutions under various boundary conditions [14–20]. The modified Sub-ODE method [21,22] provides an analytical approach for reducing nonlinear evolution equations and constructing closed-form solitary, periodic, and elliptic-function solutions.

The nonlinear Schrödinger equation also plays a fundamental role across diverse physical systems, including optical fibers, water waves, plasmas, and Bose–Einstein condensates [23–25]. In optical settings, it governs the evolution of slowly varying envelopes and models key effects such as self- and cross-phase modulation, chromatic and modal dispersion, and nonlocal interactions [26–29]. Classical studies have largely focused on deterministic (1+1)- and (2+1)-dimensional formulations under idealized assumptions, whereas higher-dimensional optical systems may also be influenced by stochastic perturbations, motivating stochastic NLS models and analyses [30–32]. Recent studies have advanced soliton perturbations using Lie symmetry [33] and quiescent vector solitons with nonlinear dispersion [34].

FBGs, characterized by periodic modulation of the refractive index along the propagation direction, provide a versatile platform for reflection, filtering, and dispersion management. In birefringent or polarization-coupled grating configurations, the optical field may be resolved into interacting orthogonally polarized components, as considered in the present model. This motivates a coupled higher-dimensional framework to investigate the combined influence of polarization interaction, spatio-temporal effects, nonlinear coupling, and stochastic perturbations in grating media.

Most Bragg-grating soliton models are traditionally posed in (1+1) dimensions, where the field envelopes depend only on the longitudinal propagation coordinate and time. Nevertheless, many contemporary FBG implementations operate in parameter ranges where genuinely spatio-temporal effects become relevant. Ultrashort and broadband pulses can develop transverse structure through diffraction/beam spreading, modal interactions, and birefringence-induced polarization coupling. Moreover, the grating response may couple to these transverse variations via spatio-temporal dispersion and higher-order nonlinear contributions. To capture such effects in a unified way, we adopt a (3+1)-dimensional description in which x denotes the principal propagation axis of the grating fiber and y and z represent transverse directions, so that the envelopes $Q(x,y,z,t)$ and $R(x,y,z,t)$ incorporate both longitudinal and transverse evolution.

This higher-dimensional formulation represents spatio-temporal solitary structures with transverse confinement, accommodates transverse modulation and distortion mechanisms arising from dispersion-diffraction interplay, and provides a generalized setting for birefringent and potentially multimode grating fibers in which orthogonally polarized components and transverse degrees of freedom co-evolve.

The mathematical structure of the (3+1)-dimensional stochastic coupled NLS framework adopted in the present study was originally introduced in Ref. [35] for birefringent optical fibers. In the present work, we consider this framework in a different physical setting, namely Fiber Bragg-grating media, where it is interpreted as a generalized effective coupled-envelope model for interacting optical field components. Therefore, the present study does not claim the original algebraic formulation of the stochastic coupled NLS system as a new contribution. Rather, the contribution lies in considering this framework within the generalized effective FBG setting and developing its analytical treatment through the modified Sub-ODE approach.

Motivated by these considerations, we consider the adopted (3+1)-dimensional coupled NLS system with explicit Itô-form white-noise terms to investigate stochastic effects in the generalized grating-fiber setting. The model incorporates higher-order dispersive effects, polarization coupling, four-wave mixing, and nonlinear interactions between orthogonal field components. To analyze this system, we employ the modified Sub-ODE method, which reduces the governing stochastic partial differential equations (SPDEs) to ordinary differential equations under an appropriate traveling-wave ansatz. This procedure yields several families of exact analytical solutions, including bright, dark, and singular solitons, as well as with periodic and elliptic-function solutions expressed in terms of Jacobi elliptic and Weierstrass $\wp$-functions.

It is important to clarify the scope of the FBG interpretation adopted in this study. In the conventional coupled-mode theory of an FBG, the periodic modulation of the refractive index couples forward- and backward-propagating envelope fields near the Bragg resonance. This coupling gives rise to a characteristic linear dispersion relation containing a photonic stop band. Nonlinear localized states whose frequencies lie inside or close to this forbidden spectral interval are conventionally referred to as gap solitons. Consequently, the grating-induced coupling coefficient and the detuning from the Bragg frequency are explicit quantities in the standard description of FBG gap solitons.

The model considered here has a different analytical focus. The system studied below is treated as a generalized effective stochastic coupled nonlinear Schrödinger envelope model motivated by birefringent/grating-fiber systems rather than as the standard forward–backward coupled-mode model of a uniform FBG. Accordingly, the present solution construction does not independently establish the conventional Bragg stop-band dispersion relation. In particular, the parameters β_j appearing in the model are interpreted as effective frequency-detuning coefficients, but their presence alone should not be regarded as a derivation of a photonic band gap.

This paper is organized as follows: Section 2 presents the adopted (3+1)-dimensional stochastic coupled NLS framework, the mathematical preliminaries, and its generalized effective interpretation in the Fiber Bragg-grating setting. Section 3 develops the analysis via a modified Sub-ODE reduction. Subsection 3.1 derives exact bright/dark, singular, and periodic/elliptic solutions with admissibility relations. Section 4 presents graphical evaluations of representative exact solutions and examines their dependence on the stochastic parameter. Section 5 presents the conclusions.

2. Mathematical preliminaries and generalized effective coupled model

The (3+1)-dimensional coupled NLS system incorporating multiplicative white noise and spatio-temporal dispersion was originally introduced in Ref. [35] to describe complex stochastic wave dynamics in birefringent optical fibers. In the present work, we consider this mathematical framework in the context of nonlinear Fiber Bragg grating media and adopt it as a generalized effective coupled-envelope model for interacting optical field components. Thus, the underlying algebraic form of the stochastic coupled NLS system is inherited from Ref. [35], whereas the present work considers its generalized effective FBG interpretation and develops the corresponding modified Sub-ODE analytical treatment.

In this interpretation, the model examines how stochasticity, higher-dimensional dispersion, polarization and intermodal interaction, four-wave mixing, and nonlinear effects influence the resulting wave structures. Accordingly, the present FBG interpretation is given by:

$$\begin{aligned} &iQ_t + a_1\left(R_{xx}+R_{yy}+R_{zz}\right) + b_1R_{xt} + c_1R_{yt} + d_1R_{zt} + \left(e_1|Q|^2 + f_1|R|^2\right)Q \\ &+\sigma\left[Q - i\left(b_1R_x + c_1R_y + d_1R_z\right)\right]\frac{dW}{dt} + i\alpha_1Q_x + \beta_1R + \delta_1Q^*R^2 \\ &= i\left[\lambda_1\left(|Q|^2Q\right)_x + \nu_1\left(|R|^2Q\right)_x + \mu_1\left(|Q|^2\right)_xQ + \theta_1\left(|R|^2\right)_xQ\right], \end{aligned} \tag{1}$$

$$\begin{aligned} &iR_t + a_2\left(Q_{xx}+Q_{yy}+Q_{zz}\right) + b_2Q_{xt} + c_2Q_{yt} + d_2Q_{zt} + \left(e_2|R|^2 + f_2|Q|^2\right)R \\ &+\sigma\left[R - i\left(b_2Q_x + c_2Q_y + d_2Q_z\right)\right]\frac{dW}{dt} + i\alpha_2R_x + \beta_2Q + \delta_2R^*Q^2 \\ &= i\left[\lambda_2\left(|R|^2R\right)_x + \nu_2\left(|Q|^2R\right)_x + \mu_2\left(|R|^2\right)_xR + \theta_2\left(|Q|^2\right)_xR\right]. \end{aligned} \tag{2}$$

In the adopted generalized effective system, $Q(x,y,z,t)$ and $R(x,y,z,t)$ denote complex-valued envelope functions that represent the interacting, orthogonally polarized components of the optical field within the present grating-fiber interpretation. These fields evolve in a four-dimensional spatio-temporal framework, where t denotes the temporal variable, x corresponds to the principal propagation direction, and y and z represent transverse directions.

A specific feature of the adopted coupled model is that the second-order and mixed spatio-temporal differential operators act on the opposite field component. Thus, derivatives of R enter the evolution equation for Q, whereas derivatives of Q enter the evolution equation for R. This cross-component structure is inherited from the generalized coupled system of Ref. [35] and is interpreted here as an effective off-diagonal dispersive coupling between the interacting optical components rather than as the conventional forward–backward Bragg-coupling mechanism.

Such a form can be represented phenomenologically by a non-diagonal linear propagation operator in the chosen modal or polarization basis, so that the dispersive evolution of one field component contributes to the evolution of the other. Accordingly, the coefficients a_j ($j = 1, 2$) characterize effective second-order cross-dispersive coupling, while b_j, c_j, and d_j characterize effective cross-component spatio-temporal coupling. A microscopic derivation of these off-diagonal terms from a particular FBG modal structure is not attempted in the present work.

The nonlinear terms $\left(e_j|Q|^2+f_j|R|^2\right)Q$ and $\left(e_j|R|^2+f_j|Q|^2\right)R$ model nonlinear refractive-index modulation due to intensity-dependent effects. Here, e_j are the self-phase modulation coefficients, while f_j account for cross-phase modulation between the interacting field components. The stochastic terms contain the coefficient σ, which quantifies the strength of the stochastic perturbation, and $dW(t)/dt$, representing the formal time derivative of a Wiener process W(t). The stochastic component is treated in the Itô sense.

The terms involving α_j correspond to intermodal dispersion and introduce asymmetry in the propagation of the interacting optical components. Here the parameters β_j are interpreted as effective frequency-detuning coefficients associated with the adopted grating-fiber envelope description. Their presence in the generalized model should not, by itself, be interpreted as establishing the conventional Bragg detuning relation or the existence of a photonic stop band. The δ_j terms describe four-wave-mixing processes involving interactions among the coupled fields and permit nonlinear energy exchange between the components.

The higher-order nonlinear terms involving spatial derivatives of nonlinear intensity products account for additional nonlinear propagation effects. The coefficients λ_j and μ_j are associated with self-steepening effects, while υ_j and θ_j represent nonlinear-dispersion contributions. Together, these terms provide an effective description of the nonlinear, dispersive, intermodal, and stochastic processes incorporated into the generalized coupled-envelope system.

The NLS-type representation employed in this work is therefore interpreted as an effective slowly varying envelope description. The present analysis takes the generalized coupled-envelope system as its mathematical starting point rather than deriving it directly from Maxwell's equations for a periodically modulated refractive-index profile. A direct first-principles FBG derivation would also require specifying the grating period and modulation depth, the forward- and backward-propagating carrier waves, the Bragg-coupling coefficient, frequency detuning, the modal or polarization basis, and the asymptotic assumptions underlying the coupled-mode reduction. This derivation differs from the exact-solution analysis pursued in the present work.

Assume that Eqs. (1) and (2) have the formal solutions:

$$
\begin{aligned}
Q(x,y,z,t)&=g_1(\xi)e^{i\left[-\kappa_1 x-\kappa_2 y-\kappa_3 z+\omega t+\sigma W(t)-\sigma^2 t\right]},\\
R(x,y,z,t)&=g_2(\xi)e^{i\left[-\kappa_1 x-\kappa_2 y-\kappa_3 z+\omega t+\sigma W(t)-\sigma^2 t\right]},
\end{aligned} \tag{3}
$$

and

$$\xi=x+y+z-vt. \tag{4}$$

It should be emphasized that the transformation (4) reduces the three spatial coordinates to a single oblique traveling coordinate. Consequently, the amplitude functions obtained below are localized with respect to ξ, but are not independently localized in the x, y and z directions. At a fixed time, the surfaces $x+y+z=constant$ form planar level sets of the amplitude. Therefore, although the governing system is formulated in a (3+1)-dimensional spacetime, the exact solutions generated through this reduction should be interpreted as multidimensional spatiotemporal traveling-wave structures rather than fully three-dimensionally localized optical bullets. Here $v,\omega,\kappa_1,\kappa_2$ and κ_3 are all non-zero parameters. The traveling coordinate ξ converts the governing PDE system into an ODE; here v is the velocity of the soliton, ω is the frequency of the soliton, $\kappa_1,\kappa_2,\kappa_3$ are the wavenumber parameters of the soliton, and $g_1(\xi)$and$g_2(\xi)$ are real functions representing the amplitude portion of the soliton. Finally, the stochastic phase term $\sigma W(t)-\sigma^2 t$, driven by the standard Wiener process $W(t)$, models white-noise-induced phase fluctuations, where the Wiener process has normally distributed increments.

If we substitute (3) and (4) into Eqs. (1) and (2) and separate the real and imaginary parts, we deduce that

$$\begin{aligned}&\left[3a_1-(b_1+c_1+d_1)v\right]g_2''+\left[-\omega+\sigma^2+\alpha_1\kappa_1\right]g_1\\&+\left[-a_1\left(\kappa_1^2+\kappa_2^2+\kappa_3^2\right)+(b_1\kappa_1+c_1\kappa_2+d_1\kappa_3)(\omega-\sigma^2)+\beta_1\right]g_2\\&+(e_1-\lambda_1\kappa_1)g_1^3+(f_1+\delta_1-\nu_1\kappa_1)g_1g_2^2=0,\end{aligned}\tag{5}$$

$$\begin{aligned}&\left[3a_2-(b_2+c_2+d_2)v\right]g_1''+\left[-\omega+\sigma^2+\alpha_2\kappa_2\right]g_2\\&+\left[-a_2\left(\kappa_1^2+\kappa_2^2+\kappa_3^2\right)+(b_2\kappa_1+c_2\kappa_2+d_2\kappa_3)(\omega-\sigma^2)+\beta_2\right]g_1\\&+(e_2-\lambda_2\kappa_1)g_2^3+(f_2+\delta_2-\nu_2\kappa_1)g_2g_1^2=0,\end{aligned}\tag{6}$$

and

$$\begin{aligned}&(\alpha_1-v)g_1'+\begin{bmatrix}-2a_1(\kappa_1+\kappa_2+\kappa_3)+(b_1+c_1+d_1)(\omega-\sigma^2)\\+(b_1\kappa_1+c_1\kappa_2+d_1\kappa_3)v\end{bmatrix}g_2'\\&-(3\lambda_1+2\mu_1)g_1^2g_1'-2(\nu_1+\theta_1)g_1g_2g_2'-\nu_1g_1'g_2^2=0,\end{aligned}\tag{7}$$

$$\begin{aligned}&(\alpha_2-v)g_2'+\begin{bmatrix}-2a_2(\kappa_1+\kappa_2+\kappa_3)+(b_2+c_2+d_2)(\omega-\sigma^2)\\+(b_2\kappa_1+c_2\kappa_2+d_2\kappa_3)v\end{bmatrix}g_1'\\&-(3\lambda_2+2\mu_2)g_2^2g_2'-2(\nu_2+\theta_2)g_1g_2g_1'-\nu_2g_2'g_1^2=0.\end{aligned}\tag{8}$$

Set

$$g_2(\xi)=\Upsilon g_1(\xi),\tag{9}$$

where Υ is a nonzero constant, provided $\Upsilon\neq1$. Now, Eqs. (5) - (8) become

$$\begin{aligned}&\left[3a_1-(b_1+c_1+d_1)v\right]\Upsilon g_1''+\begin{bmatrix}-\omega+\sigma^2+\alpha_1\kappa_1-\Upsilon a_1\left(\kappa_1^2+\kappa_2^2+\kappa_3^2\right)\\+\Upsilon(b_1\kappa_1+c_1\kappa_2+d_1\kappa_3)(\omega-\sigma^2)+\Upsilon\beta_1\end{bmatrix}g_1\\&+\left[e_1-\lambda_1\kappa_1+(f_1+\delta_1-\nu_1\kappa_1)\Upsilon^2\right]g_1^3=0,\end{aligned}\tag{10}$$

$$\begin{aligned}&\left[3a_2-(b_2+c_2+d_2)v\right]g_1''+\begin{bmatrix}(-\omega+\sigma^2+\alpha_2\kappa_2)\Upsilon-a_2\left(\kappa_1^2+\kappa_2^2+\kappa_3^2\right)\\+(b_2\kappa_1+c_2\kappa_2+d_2\kappa_3)(\omega-\sigma^2)+\beta_2\end{bmatrix}g_1\\&+\Upsilon\left[(e_2-\lambda_2\kappa_2)\Upsilon^2+f_2+\delta_2-\nu_2\kappa_1\right]g_1^3=0,\end{aligned}\tag{11}$$

and

$$\begin{aligned}&\begin{bmatrix}\alpha_1-v-2\Upsilon a_1(\kappa_1+\kappa_2+\kappa_3)+\Upsilon(b_1+c_1+d_1)(\omega-\sigma^2)\\+(b_1\kappa_1+c_1\kappa_2+d_1\kappa_3)\Upsilon v\end{bmatrix}g_1'\\&-\left[(3\lambda_1+2\mu_1)+2(\nu_1+\theta_1)\Upsilon^2+\nu_1\Upsilon^2\right]g_1^2g_1'=0,\end{aligned}\tag{12}$$

$$\begin{aligned}&\begin{bmatrix}(\alpha_2-v)\Upsilon-2a_2(\kappa_1+\kappa_2+\kappa_3)+(b_2+c_2+d_2)(\omega-\sigma^2)\\+(b_2\kappa_1+c_2\kappa_2+d_2\kappa_3)v\end{bmatrix}g_1'\\&-\Upsilon\left[(3\lambda_2+2\mu_2)\Upsilon^2+2(\nu_2+\theta_2)+\nu_2\right]g_1^2g_1'=0.\end{aligned}\tag{13}$$

Setting the coefficients of Eqs. (12) and (13) to zero, we get:

$$\alpha_1 - v - 2\Upsilon a_1(\kappa_1+\kappa_2+\kappa_3) + \Upsilon(b_1+c_1+d_1)(\omega-\sigma^2) + (b_1\kappa_1+c_1\kappa_2+d_1\kappa_3)\Upsilon v = 0, \quad (14)$$

$$(\alpha_2 - v)\Upsilon - 2a_2(\kappa_1+\kappa_2+\kappa_3) + (b_2+c_2+d_2)(\omega-\sigma^2) + (b_2\kappa_1+c_2\kappa_2+d_2\kappa_3)v = 0, \quad (15)$$

$$(3\lambda_1 + 2\mu_1) + 2(\nu_1+\theta_1)\Upsilon^2 + \nu_1\Upsilon^2 = 0, \quad (16)$$

and

$$(3\lambda_2 + 2\mu_2)\Upsilon^2 + 2(\nu_2+\theta_2) + \nu_2 = 0, \quad (17)$$

The two Eqs. (10) and (11) are equivalent if the following conditions are true:

$$\left[3a_1 - (b_1+c_1+d_1)v\right]\Upsilon = 3a_2 - (b_2+c_2+d_2)v, \quad (18)$$

$$\begin{aligned}&\left[-\omega+\sigma^2+\alpha_1\kappa_1 - \Upsilon a_1(\kappa_1^2+\kappa_2^2+\kappa_3^2) + \Upsilon(b_1\kappa_1+c_1\kappa_2+d_1\kappa_3)(\omega-\sigma^2) + \Upsilon\beta_1\right]\\ &= \left[(-\omega+\sigma^2+\alpha_2\kappa_2)\Upsilon - a_2(\kappa_1^2+\kappa_2^2+\kappa_3^2) + (b_2\kappa_1+c_2\kappa_2+d_2\kappa_3)(\omega-\sigma^2) + \beta_2\right],\end{aligned} \quad (19)$$

and

$$\left[e_1 - \lambda_1\kappa_1 + (f_1+\delta_1-\nu_1\kappa_1)\Upsilon^2\right] = \Upsilon\left[(e_2-\lambda_2\kappa_1)\Upsilon^2 + f_2 + \delta_2 - \nu_2\kappa_1\right]. \quad (20)$$

Eq. (10) can be rewritten in the form:

$$\Delta_0 g_1'' + \Delta_1 g_1 + \Delta_3 g_1^3 = 0, \quad (21)$$

where

$$\begin{aligned}\Delta_0 &= \left[3a_1 - (b_1+c_1+d_1)v\right]\Upsilon,\\ \Delta_1 &= -\omega+\sigma^2+\alpha_1\kappa_1 - \Upsilon a_1(\kappa_1^2+\kappa_2^2+\kappa_3^2) + \Upsilon(b_1\kappa_1+c_1\kappa_2+d_1\kappa_3)(\omega-\sigma^2) + \Upsilon\beta_1,\\ \Delta_3 &= e_1 - \lambda_1\kappa_1 + (f_1+\delta_1-\nu_1\kappa_1)\Upsilon^2.\end{aligned} \quad (22)$$

3. Modified sub-ODE approach

According to the modified Sub-ODE method [21,22], we now apply it to construct exact solutions of Eq. (21). The main idea is to represent the unknown amplitude function $g_1(\xi)$ as a finite series in terms of an auxiliary function $F(\xi)$ whose derivative satisfies a polynomial-type relation. In this way, Eq. (21) is transformed into an algebraic system for the unknown coefficients K_j and the auxiliary parameters π_l.

To accomplish this, we assume that Eq. (21) admits a formal solution of the form

$$g_1(\xi) = \sum_{j=0}^{h} K_j F^j(\xi), \quad (23)$$

where $K_j\,(j=0,1,2,\ldots,h)$ are constants with $K_h \neq 0$. The auxiliary function $F(\xi)$ is assumed to satisfy

$$\left[F'(\xi)\right]^2 = \pi_0 F^{2-2n}(\xi) + \pi_1 F^{2-n}(\xi) + \pi_2 F^2(\xi) + \pi_3 F^{2+n}(\xi) + \pi_4 F^{2+2n}(\xi), \quad (24)$$

where $\pi_l\,(l=0,1,2,3,4)$ are constants and n is a positive integer. This auxiliary equation is chosen because, under specific parameter selections, it generates a wide range of hyperbolic, trigonometric, Jacobi elliptic, and Weierstrass elliptic solutions. Once $F(\xi)$ is determined, $g_1(\xi)$ follows immediately from (23).

To determine the truncation index h in (23), we use the homogeneous balance principle. Let $D[\cdot]$ denote the "degree" (highest power of $g_1(\xi)$ of a term. If

$$D\left[g_1(\xi)\right] = h \text{ then } D\left[g_1'(\xi)\right] = h+n, D\left[g_1''(\xi)\right] = h+2n. \quad (25)$$

Then, more generally, the differentiation rules implied by (24) yield

$$D\left[g_1{}^{(r)}(\xi)\right]=h+rn \text{ and } D\left[g_1{}^{(r)}(\xi)g_1{}^{s}(\xi)\right]=(s+1)h+nr. \tag{26}$$

After fixing h, substituting (23) into Eq. (21) and using (24) allows Eq. (21) to be expressed as a polynomial in $F(\xi)$. Setting each polynomial coefficient to zero produces an algebraic system for the unknown constants K_j and the auxiliary parameters π_l. Solving that system provides the explicit parameter constraints under which each family of solutions exists.

It is well known [21,22] that Eq. (24) has the following solutions:

Type-1. If $\pi_0=\pi_1=\pi_3=0$, then Eq. (24) generates the solutions:

(I) The bright soliton solution:

$$\mathrm{F}(\xi)=\left[\pm\sqrt{-\frac{\pi_2}{\pi_4}}\operatorname{sech}\left(n\sqrt{\pi_2}\xi\right)\right]^{\frac{1}{n}}, \qquad \pi_2>0,\pi_4<0. \tag{27}$$

(II) The singular soliton solution:

$$\mathrm{F}(\xi)=\left[\pm\sqrt{\frac{\pi_2}{\pi_4}}\operatorname{csch}\left(n\sqrt{\pi_2}\xi\right)\right]^{\frac{1}{n}}, \qquad \pi_2>0,\pi_4>0. \tag{28}$$

(III) The periodic wave solution:

$$F(\xi)=\left[\pm\sqrt{-\frac{\pi_2}{\pi_4}}\sec\left(n\sqrt{-\pi_2}\xi\right)\right]^{\frac{1}{n}}, \qquad \pi_2\langle 0,\pi_4\rangle 0. \tag{29}$$

and

$$\mathrm{F}(\xi)=\left[\pm\sqrt{-\frac{\pi_2}{\pi_4}}\csc\left(n\sqrt{-\pi_2}\xi\right)\right]^{\frac{1}{n}}, \qquad \pi_2\langle 0,\pi_4\rangle 0. \tag{30}$$

Type-2. If $\pi_1=\pi_3=0,\pi_0=\dfrac{\pi_2^2}{4\pi_4}$, then Eq. (24) gives the solutions:

(I) The dark soliton solution:

$$\mathrm{F}(\xi)=\left[\pm\sqrt{-\frac{\pi_2}{2\pi_4}}\tanh\left(n\sqrt{-\frac{\pi_2}{2}}\xi\right)\right]^{\frac{1}{n}}, \qquad \pi_2\langle 0,\pi_4\rangle 0. \tag{31}$$

(II) The singular soliton solution:

$$\mathrm{F}(\xi)=\left[\pm\sqrt{-\frac{\pi_2}{2\pi_4}}\coth\left(n\sqrt{-\frac{\pi_2}{2}}\xi\right)\right]^{\frac{1}{n}}, \qquad \pi_2\langle 0,\pi_4\rangle 0. \tag{32}$$

(III) The periodic wave solution:

$$\mathrm{F}(\xi)=\left[\pm\sqrt{\frac{\pi_2}{2\pi_4}}\tan\left(n\sqrt{\frac{\pi_2}{2}}\xi\right)\right]^{\frac{1}{n}}, \qquad \pi_2>0,\pi_4>0. \tag{33}$$

and

$$\mathrm{F}(\xi)=\left[\pm\sqrt{\frac{\pi_2}{2\pi_4}}\cot\left(n\sqrt{\frac{\pi_2}{2}}\xi\right)\right]^{\frac{1}{n}}, \quad \pi_2>0,\pi_4>0. \tag{34}$$

Type-3. If $\pi_1=\pi_3=0$ and $0<m<1$, then Eq. (24) generates Jacobian elliptic function (JEF) solutions. The modulus parameter m controls the transition between periodic and solitary-wave limits, and the stated relations for π_0 ensure that Eq. (24) matches the standard JEF identities:

(I) When $\pi_0 = \dfrac{\pi_2^2 m^2 (m^2-1)}{\pi_4 (2m^2-1)^2}$, we have:

$$\mathrm{F}(\xi) = \left[\pm \sqrt{-\frac{\pi_2 m^2}{\pi_4 (2m^2-1)}} \mathrm{cn}\left(n\sqrt{\frac{\pi_2}{2m^2-1}}\xi \right) \right]^{\frac{1}{n}}, \quad \pi_2(2m^2-1) > 0, \pi_4 < 0. \tag{35}$$

(II) When $\pi_0 = \dfrac{\pi_2^2 (1-m^2)}{\pi_4 (2-m^2)^2}$, we have:

$$\mathrm{F}(\xi) = \left[\pm \sqrt{-\frac{\pi_2}{\pi_4 (2-m^2)}} \mathrm{dn}\left(n\sqrt{\frac{\pi_2}{2-m^2}}\xi \right) \right]^{\frac{1}{n}}, \quad \pi_2 > 0, \pi_4 < 0. \tag{36}$$

(III) When $\pi_0 = \dfrac{\pi_2^2 m^2}{\pi_4 (m^2+1)^2}$, we have:

$$\mathrm{F}(\xi) = \left[\pm \sqrt{-\frac{\pi_2 m^2}{\pi_4 (m^2+1)}} \mathrm{sn}\left(n\sqrt{-\frac{\pi_2}{m^2+1}}\xi \right) \right]^{\frac{1}{n}}, \qquad \pi_2 \langle 0, \pi_4 \rangle 0. \tag{37}$$

Type-4. If $\pi_1 = \pi_3 = 0$, then Eq. (24) yields Weierstrass elliptic function (WEF) solutions. The invariants G_2 and G_3 are determined from π_0, π_2, π_4 by matching Eq. (24) to the canonical Weierstrass equation:

(I) When $G_2 = \dfrac{4\pi_2^2 - 12\pi_0\pi_4}{3}$ and $G_3 = \dfrac{4\pi_2(-2\pi_2^2 + 9\pi_0\pi_4)}{27}$, we have:

$$\mathrm{F}(\xi) = \left[\frac{1}{\pi_4} \wp(n\xi, G_2, G_3) - \frac{\pi_2}{3\pi_4} \right]^{\frac{1}{2n}}. \tag{38}$$

and

$$\mathrm{F}(\xi) = \left[\frac{3\pi_0}{3\wp(n\xi, G_2, G_3) - \pi_2} \right]^{\frac{1}{2n}}. \tag{39}$$

(II) When $G_2 = \dfrac{\pi_2^2}{12} + \pi_0\pi_4$ and $G_3 = \dfrac{\pi_2(36\pi_0\pi_4 - \pi_2^2)}{216}$, we have:

$$\mathrm{F}(\xi) = \left[\frac{6\sqrt{\pi_0}\wp(n\xi, G_2, G_3) + \pi_2\sqrt{\pi_0}}{3\wp'(n\xi, G_2, G_3)} \right]^{\frac{1}{n}}, \tag{40}$$

and

$$\mathrm{F}(\xi) = \left[\frac{3\sqrt{\pi_4^{-1}}\wp'(n\xi, G_2, G_3)}{6\wp(n\xi, G_2, G_3) + \pi_2} \right]^{\frac{1}{n}}, \tag{41}$$

where $\wp'(n\xi, G_2, G_3) = \dfrac{d\wp(n\xi, G_2, G_3)}{d\xi}$. Here G_2 and G_3 are called invariants of the Weierstrass elliptic function. The Weierstrass elliptic function $\wp(\xi)$ and the Jacobi elliptic functions are equivalent representations of elliptic waves. If r_1, r_2, r_3 are the roots of $4u^3 - G_2 u - G_3 = 0$ (so that $(\wp')^2 = 4(\wp - r_1)(\wp - r_2)(\wp - r_3)$) and we set $m^2 = \dfrac{r_2 - r_3}{r_1 - r_3}$, then $\wp$ can be expressed in terms of the Jacobi function $\operatorname{sn}(\cdot,m)$ as $\wp(\xi)=r_3+\dfrac{r_1-r_3}{\operatorname{sn}^2\left(\sqrt{r_1-r_3}\xi,m\right)}$. Consequently, the WEF solutions in Type 4 may alternatively be rewritten in Jacobi-elliptic form, and the solitary-wave limits follow from the standard degeneracies of Jacobi functions (e.g., $m\to 1$ gives hyperbolic solitons, while $m\to 0$ yields trigonometric waves).

3.1. Soliton solutions

Based on the methodology outlined earlier, we employ the balance rule (26) to determine the appropriate form of the solution. To apply this to Eq. (21), we balance the highest derivative $g_1''(\xi)$, and the nonlinear term $g_1^3(\xi)$. The dimensional balance between these terms leads to the following condition:

$$h+2n=3h\Rightarrow h=n. \tag{42}$$

Choosing $n=1$, we obtain $h=1$. With this result, we can construct the solution to Eq. (21). This allows us to derive solutions based on the determined values of h and n. As a result, the solution to Eq. (21) can be expressed in the following form:

$$g_1(\xi)=K_0+K_1F(\xi), \tag{43}$$

where K_0 and K_1 are constants, provided $K_1\neq 0$. Substituting (43) and (24) into Eq. (21) yields the following algebraic equations:

$$\left.\begin{aligned}
&\frac{3}{2}\Delta_0K_1\pi_3+3\Delta_3K_0K_1^2=0,\\
&2\Delta_0K_1\pi_4+\Delta_3K_1^3=0,\\
&\frac{1}{2}\Delta_0K_1\pi_1+\Delta_3K_0^3+\Delta_1K_0=0,\\
&\Delta_0K_1\pi_2+3\Delta_3K_0^2K_1+\Delta_1K_1=0.
\end{aligned}\right\} \tag{44}$$

Result-1: Set $\pi_0=\pi_1=\pi_3=0$ in Eqs. (44) and solve it; one gets the result:

$$\pi_2=-\frac{\Delta_1}{\Delta_0},K_0=0,K_1=\pm\sqrt{-\frac{2\Delta_0\pi_4}{\Delta_3}}, \tag{45}$$

provided $\Delta_0\Delta_3\pi_4<0$. Substituting (45) and (27) - (30) into (43) yields the solutions for Eqs. (1) and (2) as follows:

(I) Bright soliton solutions:

$$\begin{aligned}
Q(x,\mathrm{y},\mathrm{z},t)&=\pm\sqrt{-\frac{2\Delta_1}{\Delta_3}}\\
&\quad\times\operatorname{sech}\left(\sqrt{-\frac{\Delta_1}{\Delta_0}}(x+y+z-vt)\right)\\
&\quad\times\exp\left(i\left[-\kappa_1x-\kappa_2y-\kappa_3z+\omega t+\sigma W(t)-\sigma^2t\right]\right),\\
R(x,\mathrm{y},\mathrm{z},t)&=\pm\Upsilon\sqrt{-\frac{2\Delta_1}{\Delta_3}}\\
&\quad\times\operatorname{sech}\left(\sqrt{-\frac{\Delta_1}{\Delta_0}}(x+y+z-vt)\right)\\
&\quad\times\exp\left(i\left[-\kappa_1x-\kappa_2y-\kappa_3z+\omega t+\sigma W(t)-\sigma^2t\right]\right),
\end{aligned} \tag{46}$$

provided $\Delta_1\Delta_3<0$ and $\Delta_1\Delta_0<0$.

(II) Singular soliton solutions:

$$\begin{aligned} Q(x,y,z,t) &= \pm\sqrt{2\Delta_1/\Delta_3}\operatorname{csch}\left(\sqrt{-\Delta_1/\Delta_0}\,(x+y+z-vt)\right) \\ &\quad\times\exp\left(i\left[-\kappa_1 x-\kappa_2 y-\kappa_3 z+\omega t+\sigma W(t)-\sigma^2 t\right]\right), \\ R(x,y,z,t) &= \pm\Upsilon\sqrt{2\Delta_1/\Delta_3}\operatorname{csch}\left(\sqrt{-\Delta_1/\Delta_0}\,(x+y+z-vt)\right) \\ &\quad\times\exp\left(i\left[-\kappa_1 x-\kappa_2 y-\kappa_3 z+\omega t+\sigma W(t)-\sigma^2 t\right]\right), \end{aligned} \tag{47}$$

provided $\Delta_1\Delta_3>0$ and $\Delta_1\Delta_0<0$.

(III) Periodic wave solutions:

$$\begin{aligned} Q(x,y,z,t) &= \pm\sqrt{-\frac{2\Delta_1}{\Delta_3}}\sec\left(\sqrt{\Delta_1/\Delta_0}\,(x+y+z-vt)\right) \\ &\quad\times\exp\left(i\left[-\kappa_1 x-\kappa_2 y-\kappa_3 z+\omega t+\sigma W(t)-\sigma^2 t\right]\right), \\ R(x,y,z,t) &= \pm\Upsilon\sqrt{-\frac{2\Delta_1}{\Delta_3}}\sec\left(\sqrt{\Delta_1/\Delta_0}\,(x+y+z-vt)\right) \\ &\quad\times\exp\left(i\left[-\kappa_1 x-\kappa_2 y-\kappa_3 z+\omega t+\sigma W(t)-\sigma^2 t\right]\right), \end{aligned} \tag{48}$$

and

$$\begin{aligned} Q(x,y,z,t) &= \pm\sqrt{-2\Delta_1/\Delta_3}\csc\left(\sqrt{\Delta_1/\Delta_0}\,(x+y+z-vt)\right) \\ &\quad\times\exp\left(i\left[-\kappa_1 x-\kappa_2 y-\kappa_3 z+\omega t+\sigma W(t)-\sigma^2 t\right]\right), \\ \mathrm{R}(x,y,z,t) &= \pm\Upsilon\sqrt{-2\Delta_1/\Delta_3}\csc\left(\sqrt{\Delta_1/\Delta_0}\,(x+y+z-vt)\right) \\ &\quad\times\exp\left(i\left[-\kappa_1 x-\kappa_2 y-\kappa_3 z+\omega t+\sigma W(t)-\sigma^2 t\right]\right), \end{aligned} \tag{49}$$

provided $\Delta_1\Delta_3<0$ and $\Delta_1\Delta_0>0$.

Result-2: Set $\pi_1=\pi_3=0,\pi_0=\pi_2^2/4\pi_4$ in Eqs. (44) and solve it; one gets the same result (45). If we substitute (44) and (31)-(34) into (43), we get the solutions for Eqs. (1) and (2) as follows:

(I) Dark soliton solutions:

$$\begin{aligned} Q(x,y,z,t) &= \pm\sqrt{-\frac{\Delta_1}{\Delta_3}}\tanh\left(\sqrt{\frac{\Delta_1}{2\Delta_0}}(x+y+z-vt)\right) \\ &\quad\times\exp\left(i\left[-\kappa_1 x-\kappa_2 y-\kappa_3 z+\omega t+\sigma W(t)-\sigma^2 t\right]\right), \\ R(x,y,z,t) &= \pm\Upsilon\sqrt{-\frac{\Delta_1}{\Delta_3}}\tanh\left(\sqrt{\frac{\Delta_1}{2\Delta_0}}(x+y+z-vt)\right) \\ &\quad\times\exp\left(i\left[-\kappa_1 x-\kappa_2 y-\kappa_3 z+\omega t+\sigma W(t)-\sigma^2 t\right]\right), \end{aligned} \tag{50}$$

provided $\Delta_1\Delta_3<0$ and $\Delta_1\Delta_0>0$.

(II) Singular soliton solutions:

$$\begin{aligned} Q(x,y,z,t) &= \pm\sqrt{-\frac{\Delta_1}{\Delta_3}}\coth\left(\sqrt{\frac{\Delta_1}{2\Delta_0}}(x+y+z-vt)\right) \\ &\quad\times\exp\left(i\left[-\kappa_1 x-\kappa_2 y-\kappa_3 z+\omega t+\sigma W(t)-\sigma^2 t\right]\right), \\ R(x,y,z,t) &= \pm\Upsilon\sqrt{-\frac{\Delta_1}{\Delta_3}}\coth\left(\sqrt{\frac{\Delta_1}{2\Delta_0}}(x+y+z-vt)\right) \\ &\quad\exp\left(i\left[-\kappa_1 x-\kappa_2 y-\kappa_3 z+\omega t+\sigma W(t)-\sigma^2 t\right]\right), \end{aligned} \tag{51}$$

provided $\Delta_1\Delta_3<0$ and $\Delta_1\Delta_0>0$.

(III) Periodic wave solutions:

$$Q(x,y,z,t)=\pm\sqrt{\frac{\Delta_1}{\Delta_3}}\tan\left(\sqrt{-\frac{\Delta_1}{2\Delta_0}}(x+y+z-vt)\right)\times\exp\left(i\left[-\kappa_1 x-\kappa_2 y-\kappa_3 z+\omega t+\sigma W(t)-\sigma^2 t\right]\right),$$
$$R(x,y,z,t)=\pm\Upsilon\sqrt{\frac{\Delta_1}{\Delta_3}}\tan\left(\sqrt{-\frac{\Delta_1}{2\Delta_0}}(x+y+z-vt)\right)\times\exp\left(i\left[-\kappa_1 x-\kappa_2 y-\kappa_3 z+\omega t+\sigma W(t)-\sigma^2 t\right]\right) \tag{52}$$

and

$$Q(x,y,z,t)=\pm\sqrt{\frac{\Delta_1}{\Delta_3}}\cot\left(\sqrt{-\frac{\Delta_1}{2\Delta_0}}(x+y+z-vt)\right)\times\exp\left(i\left[-\kappa_1 x-\kappa_2 y-\kappa_3 z+\omega t+\sigma W(t)-\sigma^2 t\right]\right),$$
$$R(x,y,z,t)=\pm\Upsilon\sqrt{\frac{\Delta_1}{\Delta_3}}\cot\left(\sqrt{-\frac{\Delta_1}{2\Delta_0}}(x+y+z-vt)\right)\times\exp\left(i\left[-\kappa_1 x-\kappa_2 y-\kappa_3 z+\omega t+\sigma W(t)-\sigma^2 t\right]\right) \tag{53}$$

provided $\Delta_1\Delta_3>0$ and $\Delta_1\Delta_0<0$.

Result-3: Set $\pi_1=\pi_3=0$ in Eqs. (44) and solve it; one gets the same result as in (45). If we substitute (44) and (35)-(37) into (43), we obtain the following solutions for Eqs. (1) and (2) as follows:

(I) Jacobi elliptic function solution $\mathrm{cn}(\cdot,m)$:

$$Q(x,y,z,t)=\pm m\sqrt{-\frac{2\Delta_1}{(2m^2-1)\Delta_3}}\mathrm{cn}\left(\sqrt{-\frac{\Delta_1}{(2m^2-1)\Delta_0}}(x+y+z-vt)\right)\times\exp\left(i\left[-\kappa_1 x-\kappa_2 y-\kappa_3 z+\omega t+\sigma W(t)-\sigma^2 t\right]\right)$$
$$R(x,y,z,t)=\pm m\Upsilon\sqrt{-\frac{2\Delta_1}{(2m^2-1)\Delta_3}}\mathrm{cn}\left(\sqrt{-\frac{\Delta_1}{(2m^2-1)\Delta_0}}(x+y+z-vt)\right)\times\exp\left(i\left[-\kappa_1 x-\kappa_2 y-\kappa_3 z+\omega t+\sigma W(t)-\sigma^2 t\right]\right), \tag{54}$$

provided $(2m^2-1)\Delta_1\Delta_3<0$ and $(2m^2-1)\Delta_1\Delta_0<0$.

(II) Jacobi elliptic function solution $\mathrm{dn}(\cdot,m)$:

$$Q(x,y,z,t)=\pm\sqrt{-\frac{2\Delta_1}{(2-m^2)\Delta_3}}\mathrm{dn}\left(\sqrt{-\frac{\Delta_1}{(2-m^2)\Delta_0}}(x+y+z-vt)\right)\times\exp\left(i\left[-\kappa_1 x-\kappa_2 y-\kappa_3 z+\omega t+\sigma W(t)-\sigma^2 t\right]\right),$$
$$R(x,y,z,t)=\pm\Upsilon\sqrt{-\frac{2\Delta_1}{(2-m^2)\Delta_3}}\mathrm{dn}\left(\sqrt{-\frac{\Delta_1}{(2-m^2)\Delta_0}}(x+y+z-vt)\right)\times\exp\left(i\left[-\kappa_1 x-\kappa_2 y-\kappa_3 z+\omega t+\sigma W(t)-\sigma^2 t\right]\right), \tag{55}$$

provided $\Delta_1\Delta_3<0$ and $\Delta_1\Delta_0<0$.

(III) Jacobi elliptic function solution $\mathrm{sn}(\cdot,m)$:

$$
\begin{aligned}
Q(x,y,z,t) &= \pm m\sqrt{-\frac{2\Delta_1}{(1+m^2)\Delta_3}}\,\mathrm{sn}\left(\sqrt{\frac{\Delta_1}{(1+m^2)\Delta_0}}(x+y+z-vt)\right) \\
&\quad\times\exp\left(i\left[-\kappa_1 x-\kappa_2 y-\kappa_3 z+\omega t+\sigma W(t)-\sigma^2 t\right]\right), \\
R(x,y,z,t) &= \pm m\Upsilon\sqrt{-\frac{2\Delta_1}{(1+m^2)\Delta_3}}\,\mathrm{sn}\left(\sqrt{\frac{\Delta_1}{(1+m^2)\Delta_0}}(x+y+z-vt)\right) \\
&\quad\times\exp\left(i\left[-\kappa_1 x-\kappa_2 y-\kappa_3 z+\omega t+\sigma W(t)-\sigma^2 t\right]\right),
\end{aligned} \tag{56}
$$

provided $\Delta_1\Delta_3<0$ and $\Delta_1\Delta_0>0$.

Result-4: Set $\pi_1=\pi_3=0$ in Eqs. (44) and solve it; one gets the same result (45). If we substitute (44) and (38)- (41) into (43), we obtain the following solutions for Eqs. (1) and (2) as follows:

(I) Weierstrass elliptic function solution:

$$
\begin{aligned}
Q(x,y,z,t) &= \pm\sqrt{-\frac{2}{3\Delta_3}\left[3\Delta_0\wp\left((x+y+z-vt),\frac{4\Delta_1^2-12\pi_0\pi_4\Delta_0^2}{3\Delta_0^2},\frac{8\Delta_1^3-36\pi_0\pi_4\Delta_0^2\Delta_1}{27\Delta_0^3}\right)+\Delta_1\right]} \\
&\quad\times\exp\left(i\left[-\kappa_1 x-\kappa_2 y-\kappa_3 z+\omega t+\sigma W(t)-\sigma^2 t\right]\right), \\
R(x,y,z,t) &= \pm\Upsilon\sqrt{-\frac{2}{3\Delta_3}\left[3\Delta_0\wp\left((x+y+z-vt),\frac{4\Delta_1^2-12\pi_0\pi_4\Delta_0^2}{3\Delta_0^2},\frac{8\Delta_1^3-36\pi_0\pi_4\Delta_0^2\Delta_1}{27\Delta_0^3}\right)+\Delta_1\right]} \\
&\quad\times\exp\left(i\left[-\kappa_1 x-\kappa_2 y-\kappa_3 z+\omega t+\sigma W(t)-\sigma^2 t\right]\right),
\end{aligned} \tag{57}
$$

(II) Weierstrass elliptic function solution:

$$
\begin{aligned}
Q(x,y,z,t) &= \pm\Delta_0\sqrt{\frac{-6\pi_0\pi_4}{\Delta_3\left[3\Delta_0\wp\left((x+y+z-vt),\frac{4\Delta_1^2-12\pi_0\pi_4\Delta_0^2}{3\Delta_0^2},\frac{8\Delta_1^3-36\pi_0\pi_4\Delta_0^2\Delta_1}{27\Delta_0^3}\right)+\Delta_1\right]}} \\
&\quad\times\exp\left(i\left[-\kappa_1 x-\kappa_2 y-\kappa_3 z+\omega t+\sigma W(t)-\sigma^2 t\right]\right), \\
R(x,y,z,t) &= \pm\Upsilon\Delta_0\sqrt{\frac{-6\pi_0\pi_4}{\Delta_3\left[3\Delta_0\wp\left((x+y+z-vt),\frac{4\Delta_1^2-12\pi_0\pi_4\Delta_0^2}{3\Delta_0^2},\frac{8\Delta_1^3-36\pi_0\pi_4\Delta_0^2\Delta_1}{27\Delta_0^3}\right)+\Delta_1\right]}} \\
&\quad\times\exp\left(i\left[-\kappa_1 x-\kappa_2 y-\kappa_3 z+\omega t+\sigma W(t)-\sigma^2 t\right]\right),
\end{aligned} \tag{58}
$$

(III) Weierstrass elliptic function solution:

$$
\begin{aligned}
Q(x,y,z,t) &= \pm\sqrt{-\frac{2\pi_0\pi_4\Delta_0}{\Delta_3}}\left[\frac{6\Delta_0\wp\left((x+y+z-vt),\frac{\Delta_1^2+12\pi_0\pi_4\Delta_0^2}{12\Delta_0^2},\frac{\Delta_1^3-36\pi_0\pi_4\Delta_0^2\Delta_1}{216\Delta_0^3}\right)-\Delta_1}{3\Delta_0\wp'\left((x+y+z-vt),\frac{\Delta_1^2+12\pi_0\pi_4\Delta_0^2}{12\Delta_0^2},\frac{\Delta_1^3-36\pi_0\pi_4\Delta_0^2\Delta_1}{216\Delta_0^3}\right)}\right] \\
&\quad\times\exp\left(i\left[-\kappa_1 x-\kappa_2 y-\kappa_3 z+\omega t+\sigma W(t)-\sigma^2 t\right]\right), \\
R(x,y,z,t) &= \pm\Upsilon\sqrt{-\frac{2\pi_0\pi_4\Delta_0}{\Delta_3}}\left[\frac{6\Delta_0\wp\left((x+y+z-vt),\frac{\Delta_1^2+12\pi_0\pi_4\Delta_0^2}{12\Delta_0^2},\frac{\Delta_1^3-36\pi_0\pi_4\Delta_0^2\Delta_1}{216\Delta_0^3}\right)-\Delta_1}{3\Delta_0\wp'\left((x+y+z-vt),\frac{\Delta_1^2+12\pi_0\pi_4\Delta_0^2}{12\Delta_0^2},\frac{\Delta_1^3-36\pi_0\pi_4\Delta_0^2\Delta_1}{216\Delta_0^3}\right)}\right] \\
&\quad\times\exp\left(i\left[-\kappa_1 x-\kappa_2 y-\kappa_3 z+\omega t+\sigma W(t)-\sigma^2 t\right]\right),
\end{aligned} \tag{59}
$$

(IV) Weierstrass elliptic function solution:

$$\begin{aligned}
Q(x,y,z,t) &= \pm\sqrt{-\frac{2\Delta_0}{\Delta_3}} \\
&\times\left[\frac{3\Delta_0\wp'\left((x+y+z-vt),\dfrac{\Delta_1^2+12\pi_0\pi_4\Delta_0^2}{12\Delta_0^2},\dfrac{\Delta_1^3-36\pi_0\pi_4\Delta_0^2\Delta_1}{216\Delta_0^2}\right)}{6\Delta_0\wp\left((x+y+z-vt),\dfrac{\Delta_1^2+12\pi_0\pi_4\Delta_0^2}{12\Delta_0^2},\dfrac{\Delta_1^3-36\pi_0\pi_4\Delta_0^2\Delta_1}{216\Delta_0^3}\right)-\Delta_1}\right] \\
&\times\exp\left(i\left[-\kappa_1 x-\kappa_2 y-\kappa_3 z+\omega t+\sigma W(t)-\sigma^2 t\right]\right), \\
R(x,y,z,t) &= \pm\Upsilon\sqrt{-\frac{2\Delta_0}{\Delta_3}} \\
&\times\left[\frac{3\Delta_0\wp'\left((x+y+z-vt),\dfrac{\Delta_1^2+12\pi_0\pi_4\Delta_0^2}{12\Delta_0^2},\dfrac{\Delta_1^3-36\pi_0\pi_4\Delta_0^2\Delta_1}{216\Delta_0^2}\right)}{6\Delta_0\wp\left((x+y+z-vt),\dfrac{\Delta_1^2+12\pi_0\pi_4\Delta_0^2}{12\Delta_0^2},\dfrac{\Delta_1^3-36\pi_0\pi_4\Delta_0^2\Delta_1}{216\Delta_0^3}\right)-\Delta_1}\right] \\
&\times\exp\left(i\left[-\kappa_1 x-\kappa_2 y-\kappa_3 z+\omega t+\sigma W(t)-\sigma^2 t\right]\right).
\end{aligned} \tag{60}$$

4. Physical interpretation of soliton solutions

Soliton solutions play a fundamental role in nonlinear science, describing stable, localized structures that emerge from the balance between dispersion and nonlinearity. Depending on the type of solution, solitons can represent either localized wave packets (bright solitons) or topological transitions (dark solitons). Understanding their physical meaning provides insight into how deterministic and stochastic effects shape their amplitude, width, velocity, and stability. In this section, we analyze and compare the physical behavior of bright soliton and dark soliton solutions.

The figures presented in this section are graphical evaluations of the exact analytical solutions derived above. For ($\sigma\neq 0$), representative realizations of the standard Wiener process $W(t)$ are generated and substituted into the stochastic phase of the analytical expressions. These graphical realizations illustrate the dependence of the resulting wave profiles on the stochastic parameter and should not be interpreted as independent numerical validation of the original stochastic PDE system.

4.1. Bright soliton solution

The sech-type solution represents a bright soliton, a localized bell-shaped wave that smoothly decays to zero at spatial infinity. Physically, the amplitude defines the soliton's height, the inverse width determines its degree of localization, and the velocity controls its drift through the medium. In addition, the complex exponential phase factor introduces oscillatory modulation into the real and imaginary components of the field. For the graphical illustrations, the transverse coordinates are fixed at $y = 0$ and $z = 0$, so that the analytical solution is displayed in the (x)–(t) plane. The remaining parameters are taken as $a_1=1, b_1=0.2, c_1=0.2, d_1=0.2, \alpha_1=1.5, \beta_1=0.8, \kappa_1=0.3, \kappa_2=0.3, \kappa_3=0.3, \Upsilon=1.2, \omega=1.4, e_1=1,$ $f_1=1, \delta_1=0.5, \nu_1=0.5, \lambda_1=0.5, \mu_1=1, \theta_1=-1.96$ and $W(t)$ denotes a standard Wiener process with $W(0) = 0$ and increments $W(t+\Delta t)-W(t)\sim\mathcal{N}(0,\Delta t)$. Representative stochastic realizations of $W(t)$ are generated accordingly to evaluate the analytical solution.

In Fig. 1 ($\sigma = 0$), the bright soliton appears broad and smooth, with relatively small amplitude (≈0.9) and very slow drift ($v \approx 0.44$), representing a stable deterministic pulse in the absence of noise. In Fig. 2 ($\sigma = 1$), the amplitude grows (≈ 0.30), the width narrows, and the velocity increases significantly in magnitude ($v \approx -4.3$), producing a sharper and faster pulse. The stronger oscillatory modulation in the field reflects the impact of moderate stochasticity. In Fig. 3 ($\sigma = 5$) the soliton becomes extremely narrow and highly localized with a characteristic width (≈ 0.21) along the reduced traveling coordinate and propagates with an ultra-large velocity ($v \approx -106$). The waveforms exhibit stronger modulation and reduced coherence in the simulated realizations.

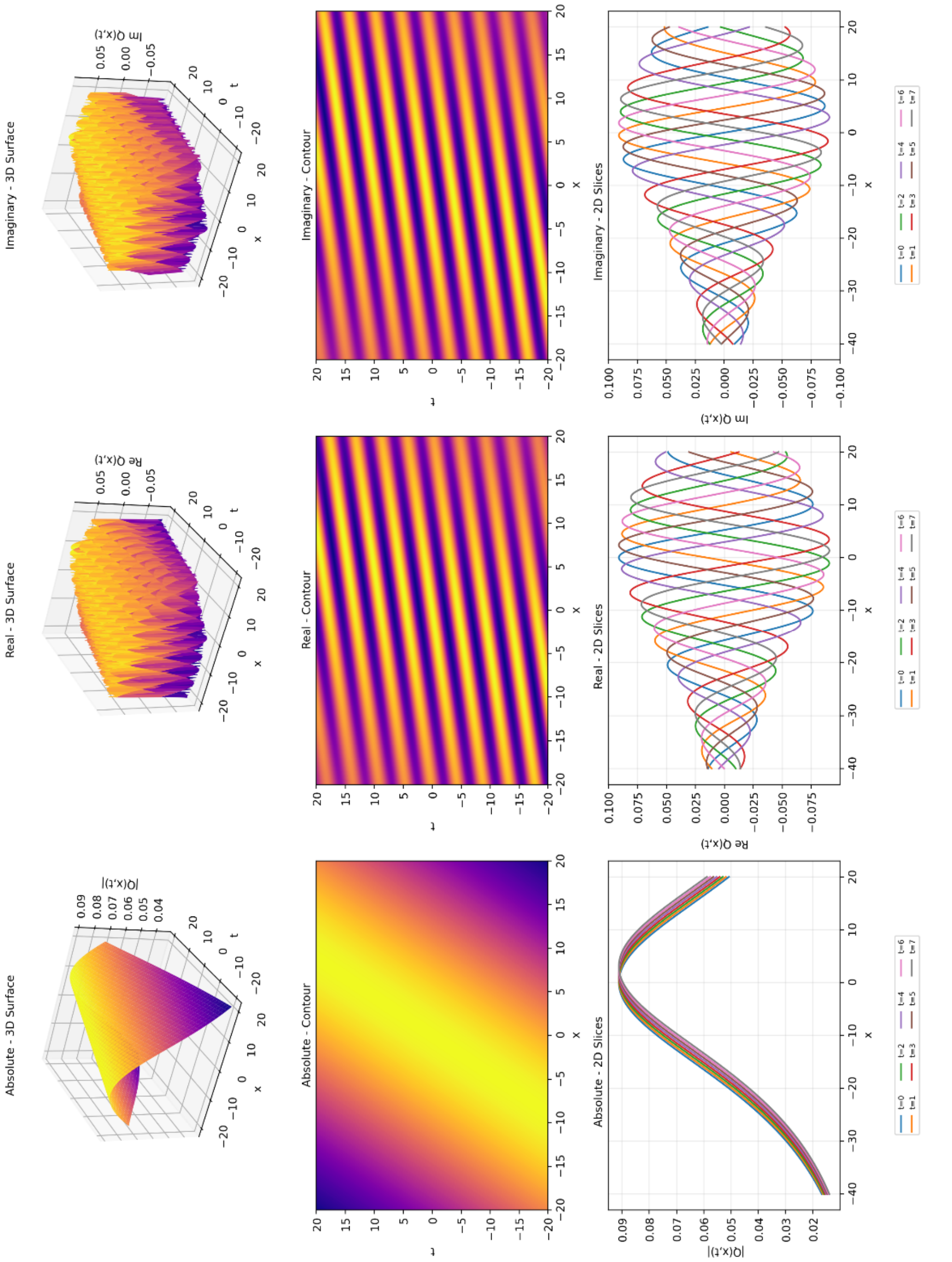

Fig. 1. Bright soliton solution (46) for $\sigma = 0$, $v \approx 0.44$, showing a smooth, stable localized pulse with weak oscillations and slow drift in the deterministic, noise-free case.

These results show that, for the selected parameter sets, increasing σ is associated with stronger localization, faster propagation, and enhanced oscillatory modulation of the bright solitary-wave profiles. In nonlinear optical systems, such localized structures are of interest for understanding wave propagation in dispersive and nonlinear media. The present results specifically illustrate how the stochastic contribution modifies the characteristics of the bright analytical solitary-wave solutions within the considered coupled model. This underscores the versatility of the bright soliton model across diverse physical systems and illustrates how the noise intensity σ can alter the observed waveform structure, modulation, and coherence as the dynamics move away from the purely deterministic regime.

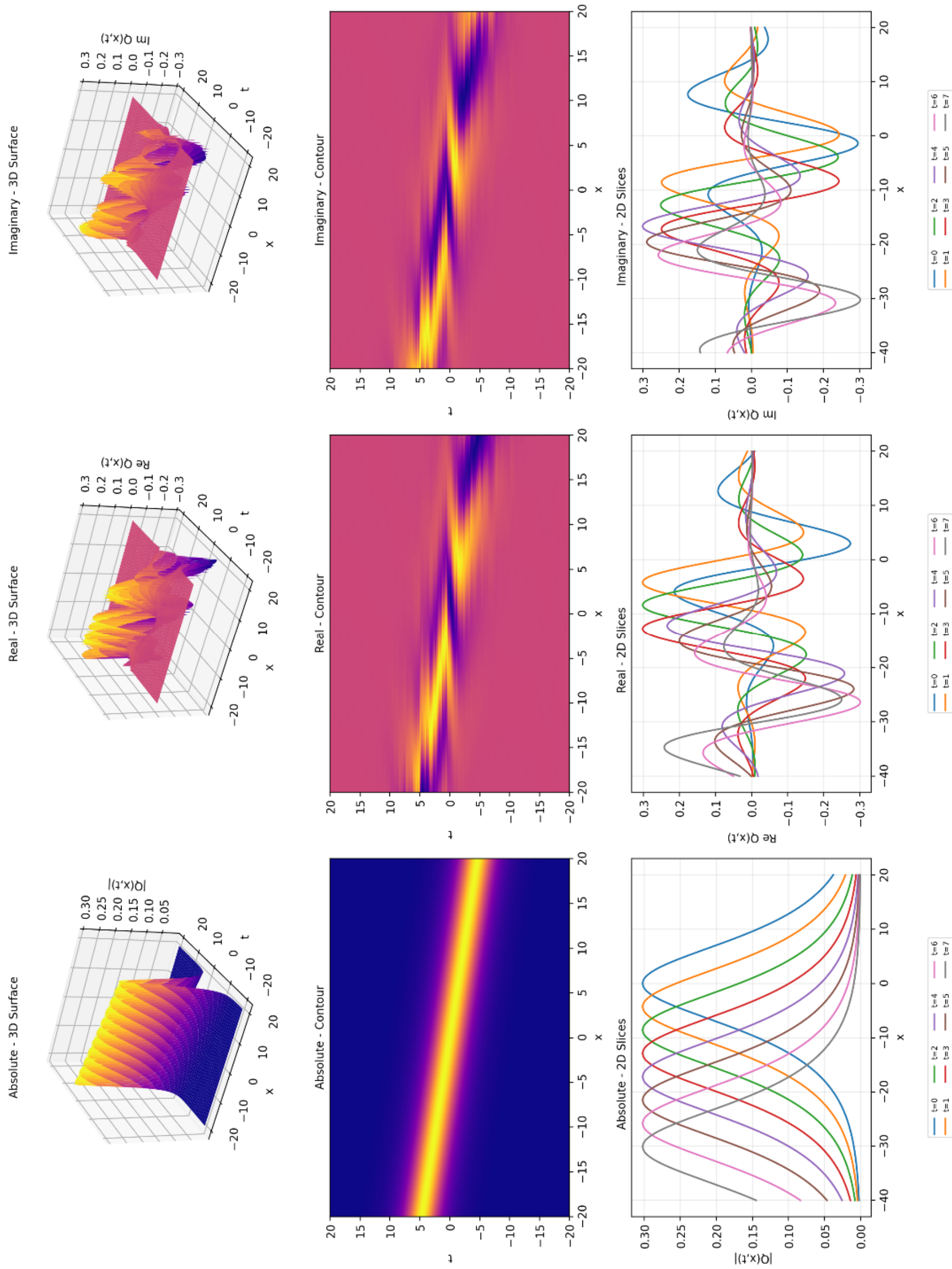

Fig. 2. Bright soliton solution (46) for $\sigma = 1$, $\nu \approx -4.3$, showing a sharper, higher-amplitude localized pulse with stronger oscillations and faster drift, corresponding to a stochastically driven soliton under moderate noise.

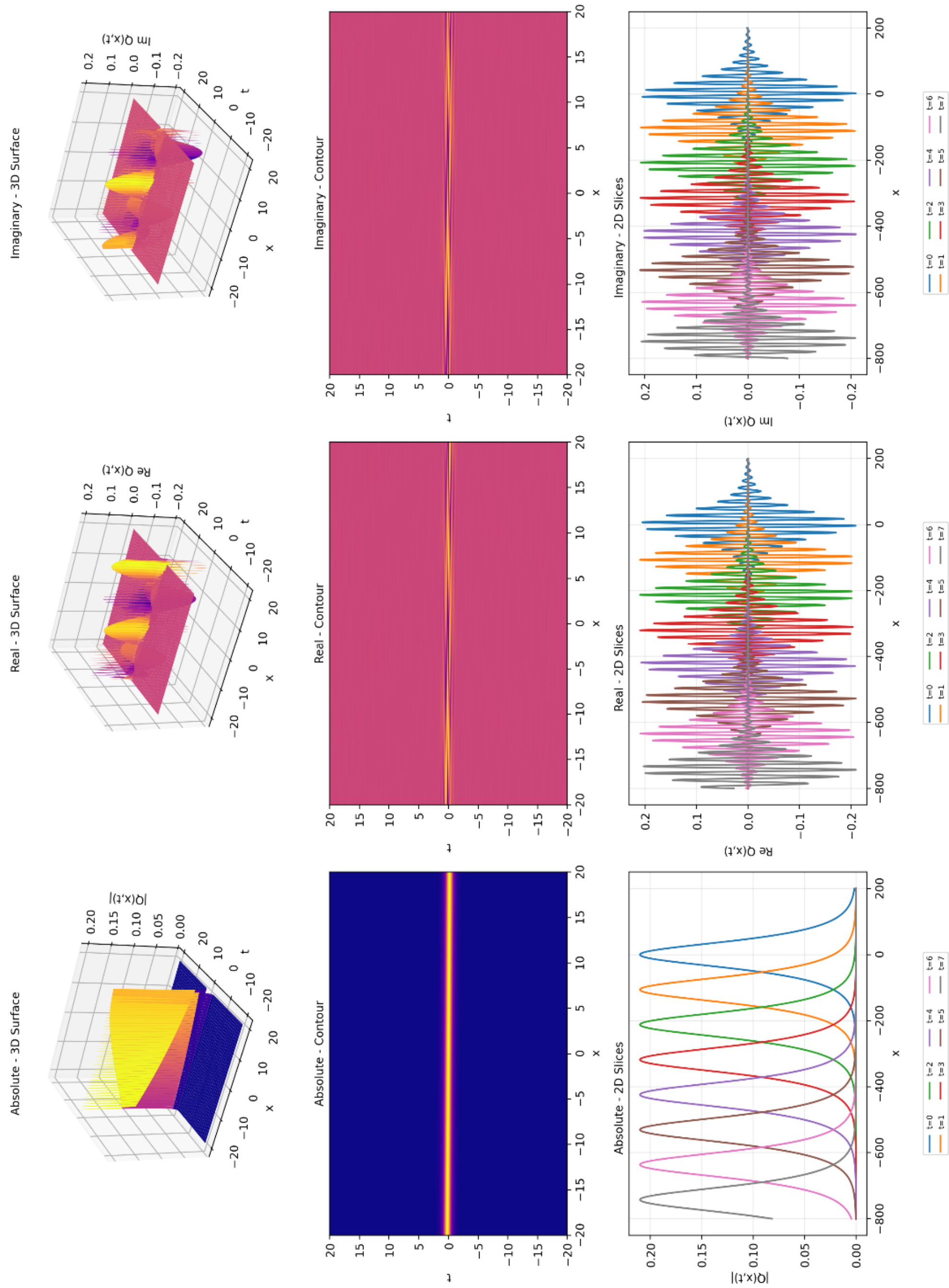

Fig. 3. Bright soliton solution (46) for $\sigma = 5, \nu \approx -106$, showing a steep, spike-like envelope with rapid oscillations, strong modulation, and ultra-fast drift, representing a highly unstable, noise-dominated soliton.

4.2. Dark soliton solution

Figs. 4-6 present the dark soliton at increasing stochastic strength. For the graphical illustrations, the transverse coordinates are fixed at $y = 0$ and $z = 0$, so that the analytical solution is displayed in the $(x)-(t)$ plane. The system parameters are $a_1 = 1, b_1 = 0.2, c_1 = 0.2$, $d_1 = 0.2, \alpha_1 = 1.5, \beta_1 = 0.8, \kappa_1 = 0.3, \kappa_2 = 0.3, \kappa_3 = 0.3, \omega = 1.4, e_1 = 1, f_1 = 1, \delta_1 = -2, \nu_1 = 0.5, \lambda_1 = 0.5$, $\mu_1 = 1, \theta_1 = -1.96$ and $W(t)$ denotes a standard Wiener process with $W(0) = 0$ and increments $W(t + \Delta t) - W(t) \sim \mathcal{N}(0, \Delta t)$. In numerical illustrations, stochastic realizations of

$W(t)$ are generated accordingly. The results are shown for Fig. 4 with $\sigma=0, \Upsilon=2, v=-0.66$, Fig. 5 with $\sigma=1, \Upsilon=2, v=-7.22$, and Fig. 6 with $\sigma=5, \Upsilon=1.1, v=-150$, each displaying the envelope $|Q(x,t)|$ alongside its real and imaginary parts.

At $\sigma=0$ (Fig. 4), the envelope forms a broad, smooth kink of moderate amplitude with very slow drift, while $\Re Q$ and $\Im Q$ exhibit weak and smooth oscillations aligned with the propagating front, characteristic of a deterministic domain-wall (dark-soliton) profile. This corresponds to an ideal dark soliton, commonly encountered in optical fibers, Bose-Einstein condensates, and magnetic spin chains, where coherence is maintained in the absence of noise.

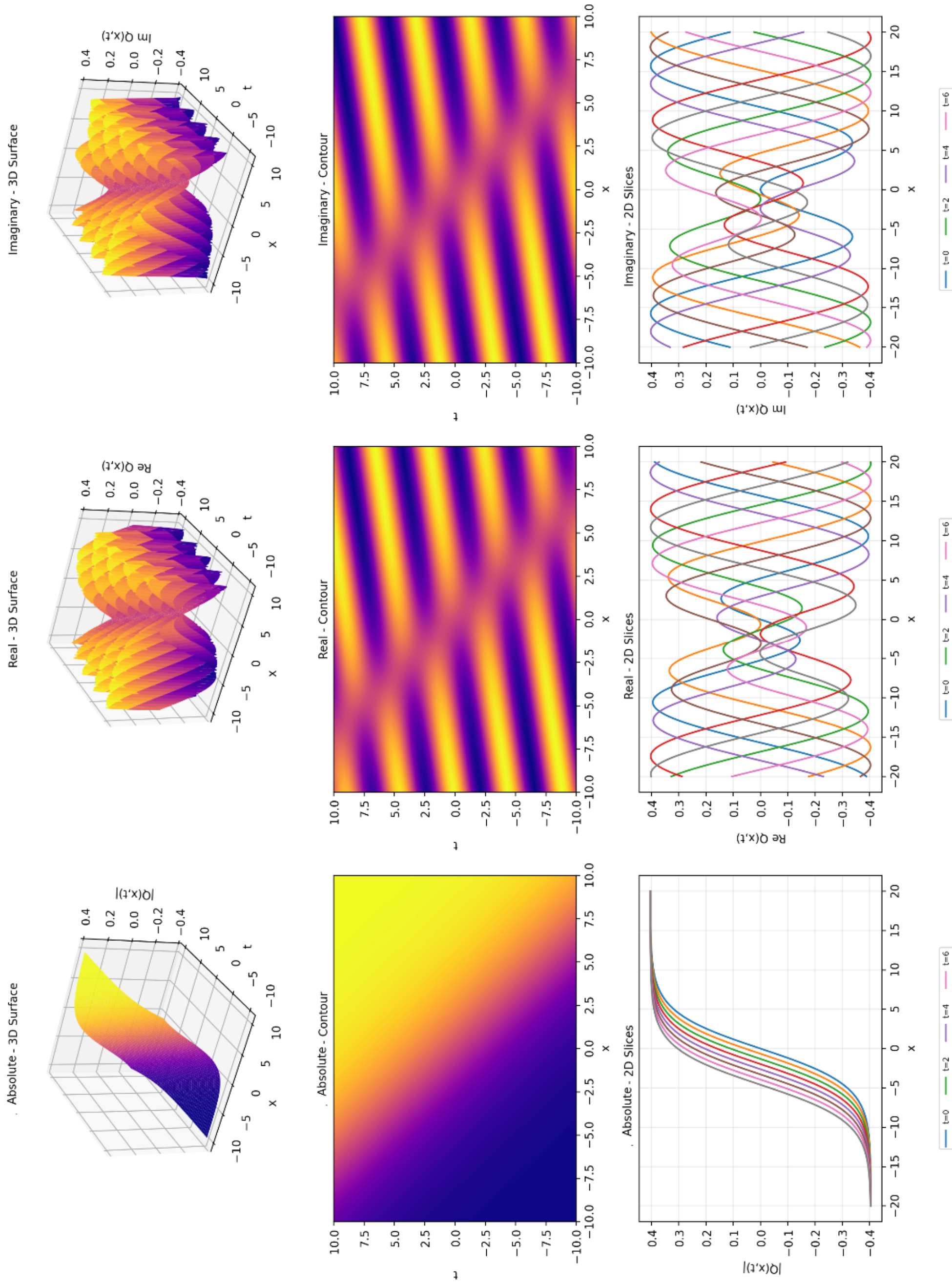

Fig. 4. Dark soliton solution (50) for $\sigma=0$, showing a broad, smooth kink with very slow drift and weak oscillations in Re Q and Im Q, representing a stable deterministic domain wall.

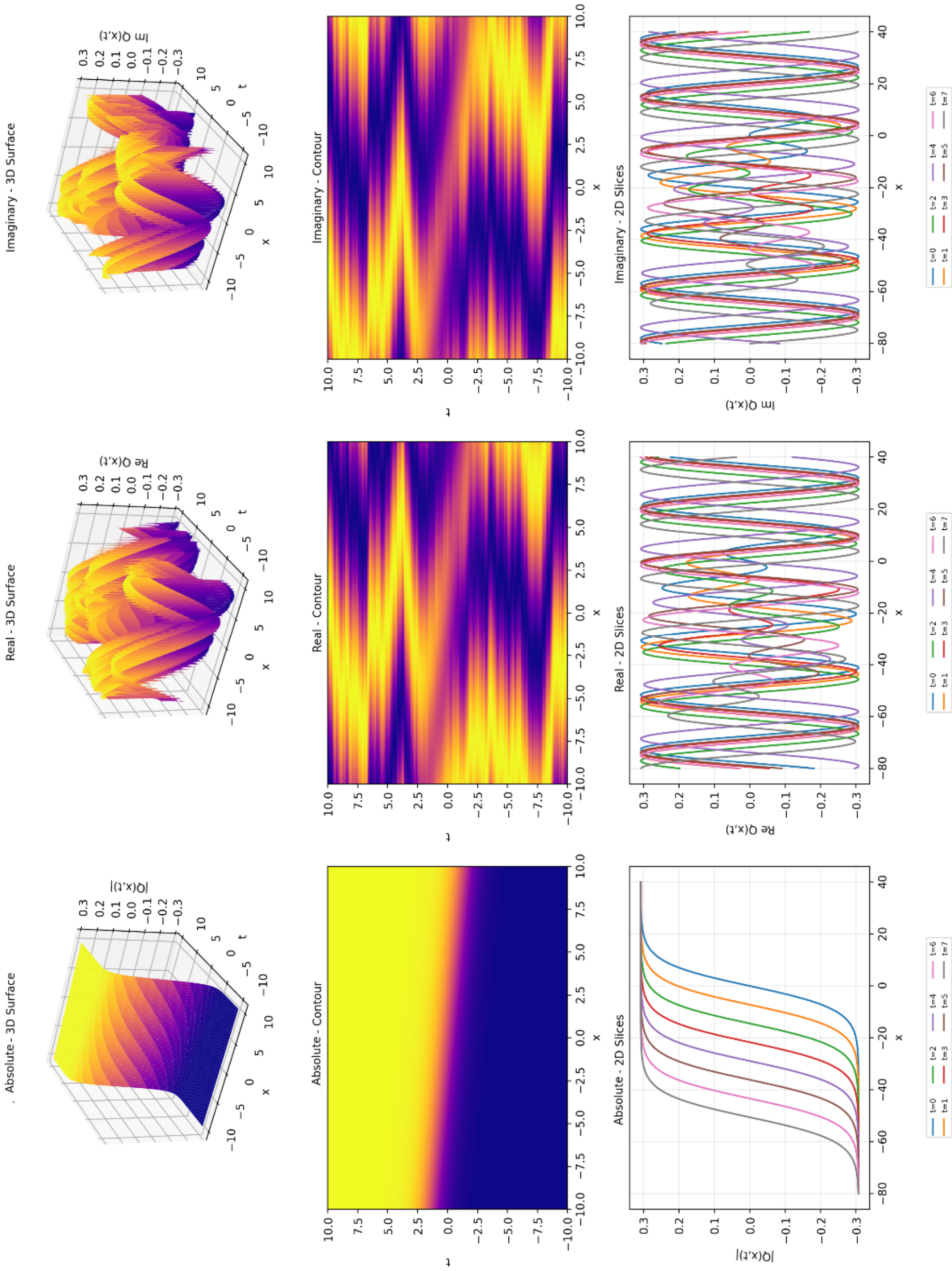

Fig. 5. Dark soliton solution (50) for $\sigma = 1$, showing a sharper, faster-drifting front with slightly reduced amplitude, where $\operatorname{Re} Q$ and $\operatorname{Im} Q$ display stronger oscillatory modulation from the stochastic phase, representing a moderately stochastic

At $\sigma = 1$ (Fig. 5), the front sharpens and drifts faster; the envelope becomes more localized with slightly reduced amplitude, and both $\operatorname{Re} Q$ and $\operatorname{Im} Q$ exhibit stronger oscillatory modulation due to the stochastic phase. Compared with the deterministic case, the graphical profile shows how including a moderate stochastic parameter modifies the propagation and phase characteristics of the analytical dark solitary-wave solution.

At $\sigma = 5$ (Fig. 6), the front becomes nearly step-like with large amplitude and ultra-fast propagation, while $\operatorname{Re} Q$ and $\operatorname{Im} Q$ become highly oscillatory and tightly coupled to the steep interface. Compared with the lower-σ cases, this graphical realization illustrates a pronounced influence of the stochastic phase contribution on the shape and propagation characteristics of the analytical dark solitary-wave solution.

Overall, increasing σ sharpens the front, increases the apparent propagation rate in the displayed realizations, and enhances the phase-induced modulation of the dark soliton. Physically, this shows how noise intensity can drive the dynamics away from the purely deterministic domain-wall regime toward a more strongly noise-influenced switching front, with implications for optical communication systems, control of condensate dynamics, and modeling stochastic transport in complex media.

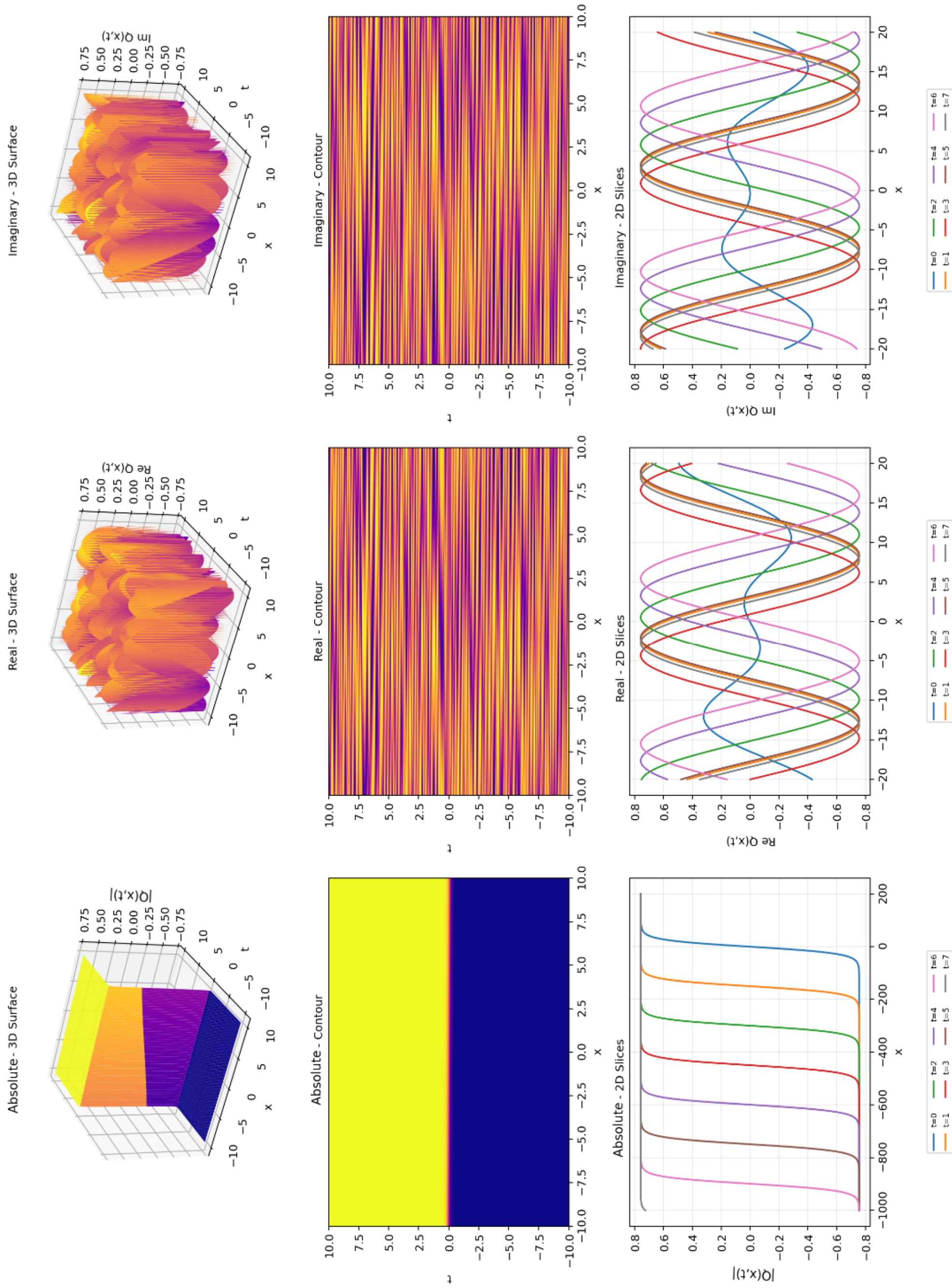

Fig. 6. Dark soliton solution (50) for $\sigma = 5$, showing a nearly step-like front with large amplitude and ultra-fast propagation, where Re Q and Im Q are highly oscillatory and coupled to the steep interface, indicating strongly modulated, noise-dominated dynamics.

4.3. Jacobi elliptic solution

In addition to the hyperbolic soliton families, the coupled stochastic system also supports the Jacobi elliptic function solution. In addition, the complex exponential phase factor introduces oscillatory modulation into the real and imaginary components of the field. For the graphical illustrations, the transverse coordinates are fixed at $y = 0$ and $z = 0$, so that the analytical solution is displayed in the $(x)-(t)$ plane. Here the parameters are taken as $a_1 = 1, b_1 = 0.2$, $c_1 = 0.2, d_1 = 0.2, \alpha_1 = 1.5, \beta_1 = 0.8, \kappa_1 = 0.3, \kappa_2 = 0.3, \kappa_3 = 0.3, \Upsilon = 1.2, \omega = 1.4, e_1 = 1, f_1 = 1, \delta_1 = 0.5$, $\nu_1 = 0.5, \lambda_1 = 0.5, \mu_1 = 1, \theta_1 = -1.96, m = 0.8$ and $W(t)$ denotes a standard Wiener process with

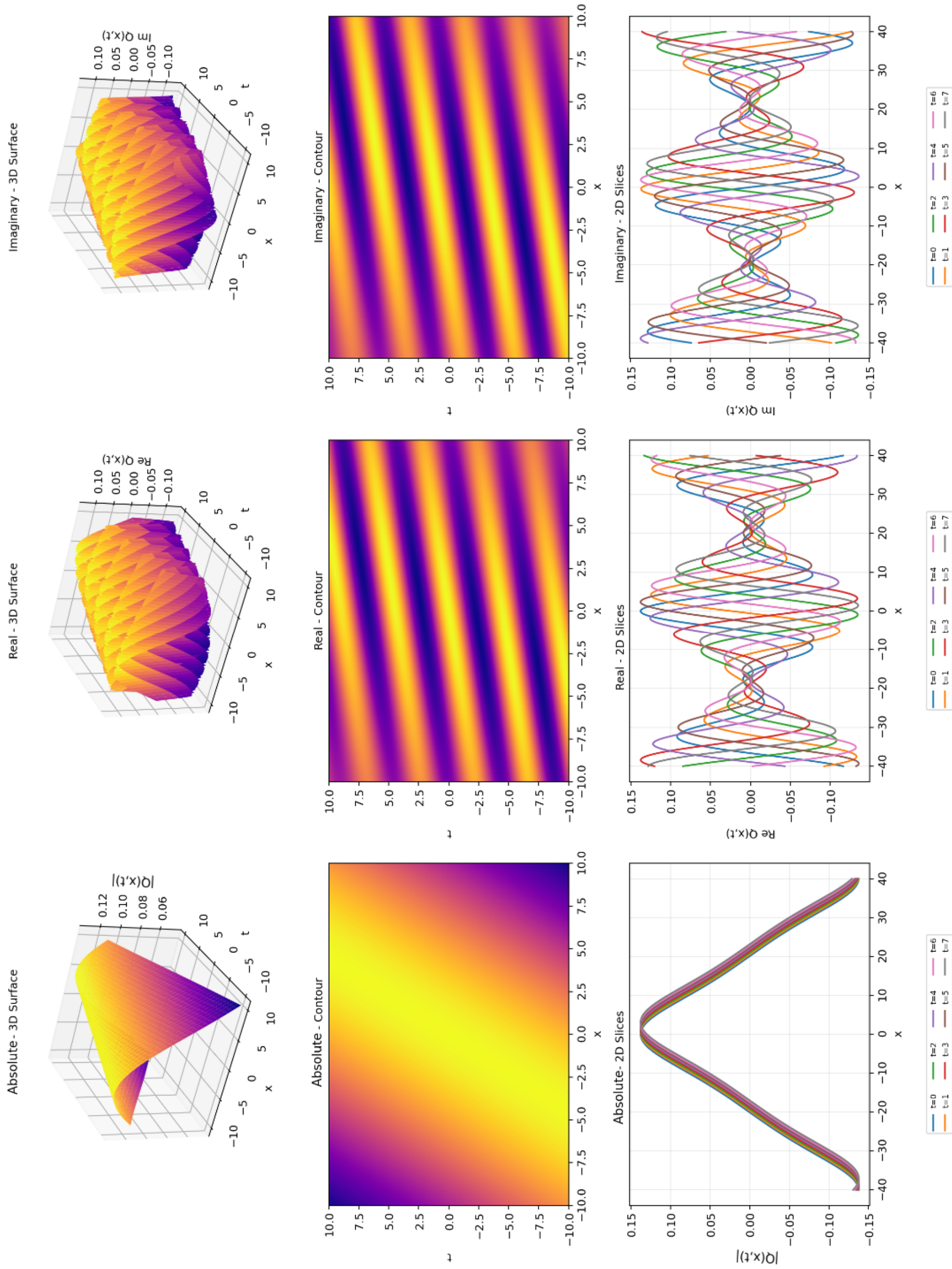

Fig. 7. Jacobi solution (54) for $\sigma = 0$, showing coherent cnoidal-wave propagation (envelope, real and imaginary parts) in the deterministic regime.

$W(0) = 0$ and increments $W(t+\Delta t) - W(t) \sim \mathcal{N}(0, \Delta t)$. In numerical illustrations, stochastic realizations of $W(t)$ are generated accordingly. The admissibility conditions of Eq. (54) ensure real-valued amplitude and physically meaningful propagation under the balance between dispersion and nonlinear response.

Figs. 7-9 illustrate the dynamical features of the Jacobi cn-solution (54) for three noise strengths $\sigma = 0,1,5$ (showing the envelope $|Q(x,t)|$ together with $\mathrm{Re}\,Q$ and $\mathrm{Im}\,Q$ via 3D surfaces, contours, and representative 2D slices). For $\sigma = 0$ (Fig. 7), the envelope exhibits a smooth, weakly modulated cnoidal structure with comparatively small amplitude, while $\mathrm{Re}\,Q$

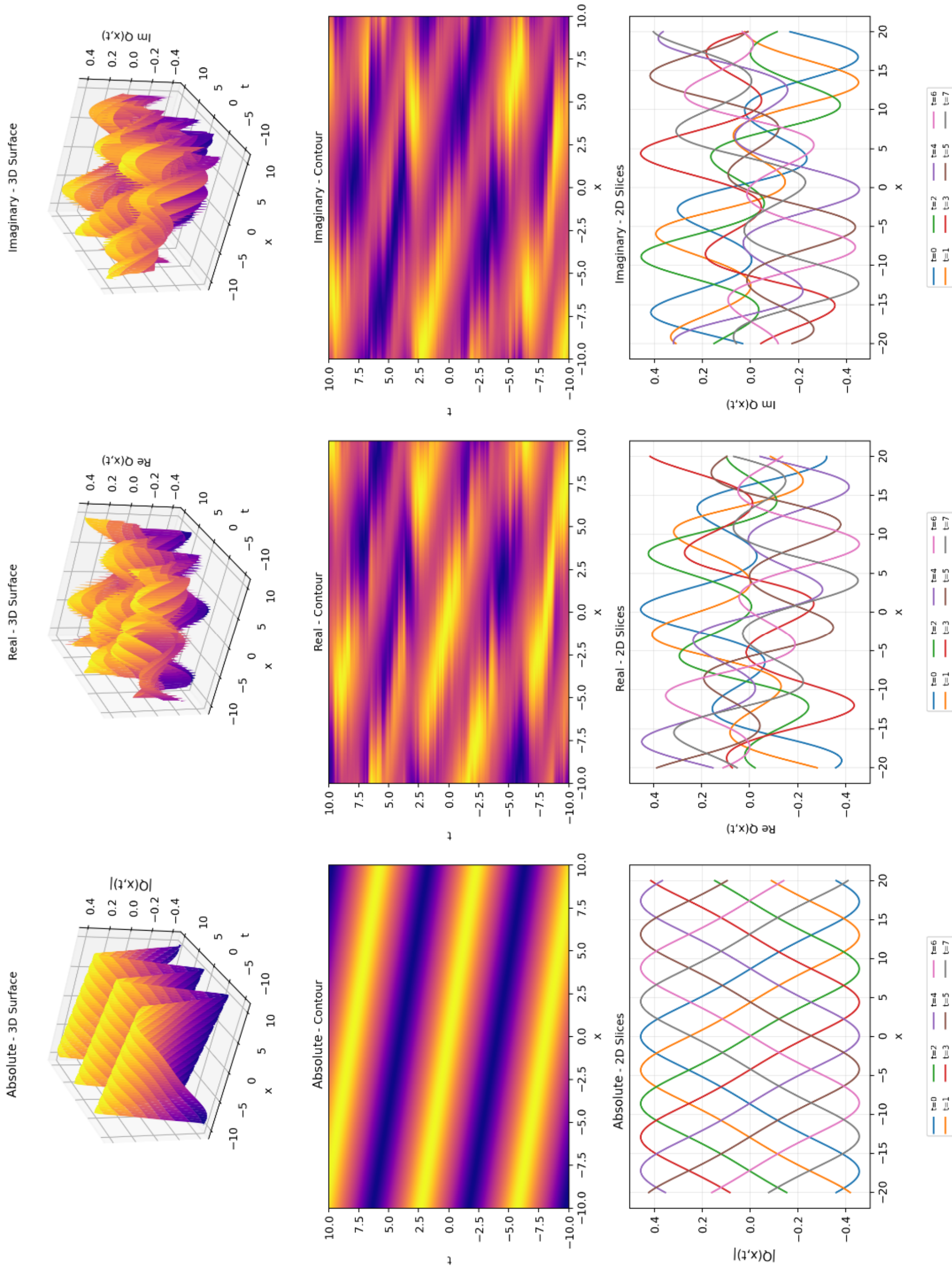

Fig. 8. Jacobi solution (54) for $\sigma = 1$, showing enhanced modulation and stronger periodic ridges due to moderate stochasticity.

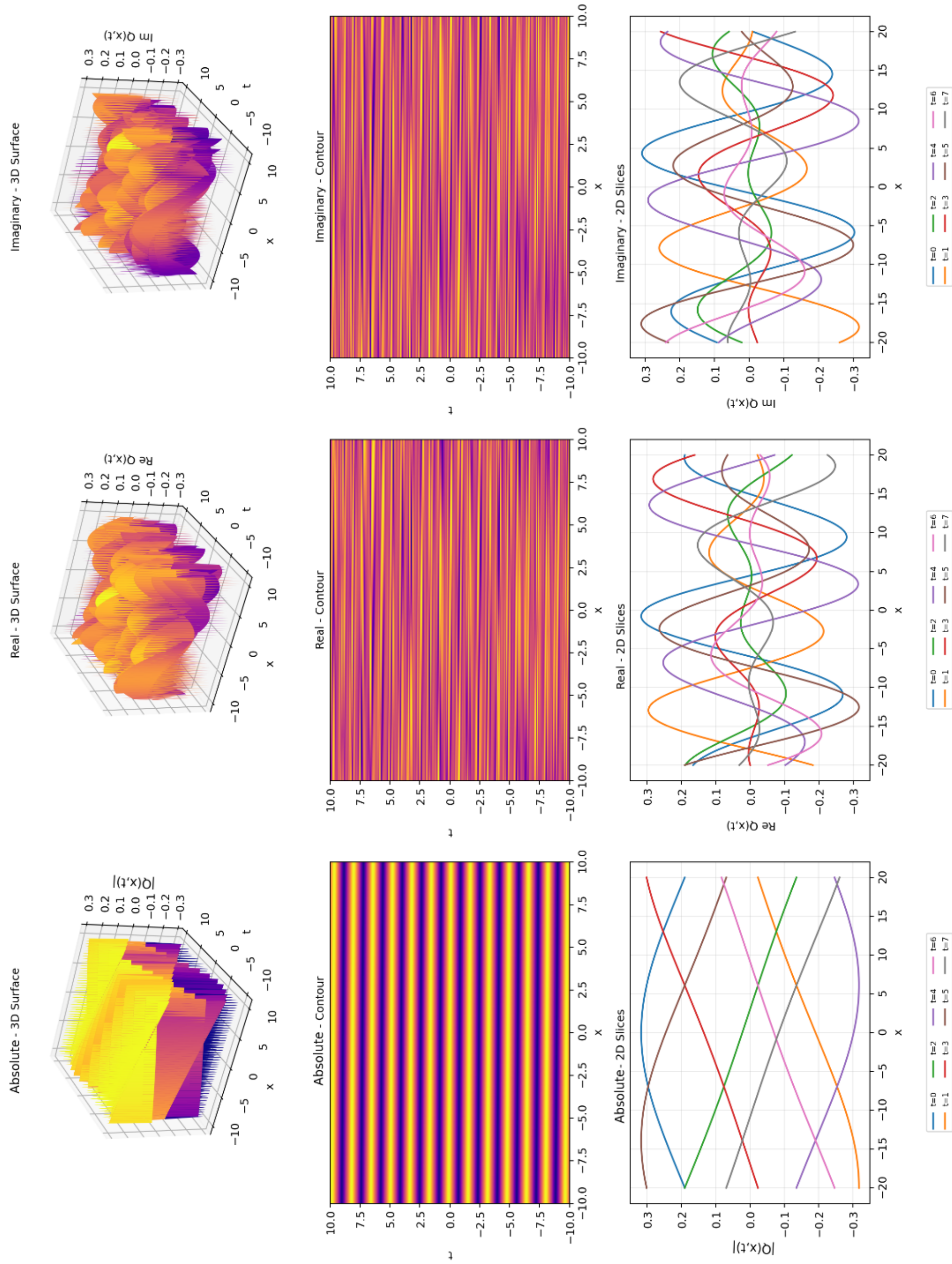

Fig. 9. Jacobi solution (54) for $\sigma = 5$, showing strongly distorted, noise-dominated cnoidal dynamics with sharp crests and dense contour stripes.

and Im Q display regular oscillations associated with the deterministic phase evolution, indicating a coherent periodic traveling wave. As the noise intensity increases to $\sigma = 1$ (Fig. 8), the oscillatory character becomes more pronounced: the envelope develops stronger periodic ridges and the real/imaginary components show enhanced modulation (phase jitter), reflecting the fact that stochasticity modifies the effective parameters entering the wavenumber and amplitude through the coefficients in the reduced model. For strong noise $\sigma = 5$ (Fig. 9), the waveform becomes highly corrugated with sharper crests and denser stripe patterns in the contour plots, signaling a noise-dominated regime where the periodic train persists but experiences strong distortion and rapid modulation in Re Q and Im Q. This behavior parallels the general role of stochasticity that means increasing σ intensifies oscillatory modulation and can drive the system from a coherent deterministic regime toward strongly fluctuating dynamics.

From a physical standpoint, Jacobi elliptic waves model in fiber Bragg gratings are relevant in photonic signal generation, optical filtering, and pattern formation. The results in Figs. 7-9 demonstrate that multiplicative white noise does not merely perturb the phase: it can substantially reshape the effective amplitude and spatio-temporal modulation of the cnoidal waveform, thereby influencing stability, coherence, and the transition between near-soliton and strongly periodic regimes.

5. Conclusions

We have investigated a (3+1)-dimensional stochastic coupled NLS system within a generalized effective Fiber Bragg-grating envelope framework and analyzed its soliton dynamics using the modified Sub-ODE method. The mathematical structure of the governing stochastic coupled NLS system was originally introduced in Ref. [35] for birefringent optical fibers; in the present work, we consider this framework in the FBG setting as a generalized effective coupled-envelope model for interacting optical field components. Accordingly, the novelty of the present study lies not in the original formulation of the governing system itself, but in its generalized effective FBG interpretation, together with the modified Sub-ODE reduction and the associated analytical solution construction. We derived a broad class of exact analytical solutions, including bright solitons, dark solitons, singular solitons, and periodic structures, as well as solutions expressed in terms of Jacobi and Weierstrass elliptic functions. The results show that stochastic perturbations can markedly affect observed soliton features, including envelope amplitude and width, apparent waveform drift in representative realizations, and phase-induced modulation of the complex field components. Overall, the present analysis establishes several families of exact soliton and periodic solutions for the considered (3+1)-dimensional stochastic coupled NLS system and illustrates how the stochastic parameter enters their phase and modifies the displayed wave profiles under the selected parameter sets. The results provide an analytical framework for examining the interplay among nonlinear coupling, dispersion, and stochastic effects in the adopted coupled-envelope model. Independent numerical integration of the governing stochastic PDE system and ensemble-based statistical characterization remain natural directions for further investigation. Such studies would provide a useful basis for assessing the robustness of the exact analytical solutions under stochastic evolution and for further evaluating the applicability and limitations of the generalized effective FBG interpretation adopted here.

Funding and acknowledgment. Ongoing Research Funding Program (ORF-RICSP-2026-9), King Saud University, Riyadh, Saudi Arabia. This research, for the last author, was supported by Grambling State University for the Endowed Chair of Mathematics and is gratefully appreciated.

Author Contributions. Ahmed S. M. Metwally: Conceptualization, methodology, formal analysis, investigation. Mohamed E. M. Alngar: Validation, methodology, data curation, writing–original paper, writing–review & editing. Reham M. A. Shohib: Formal analysis, supervision, validation, investigation, writing–review & editing. Sagar E. Shirsath: Methodology, software, visualization, validation. Anjan Biswas: Conceptualization, supervision, methodology, validation, funding. All authors have read and agreed to the published version of the manuscript.

Conflict of interest. The authors declare no conflict of interest.

References

1. Eggleton, B. J., Slusher, R. E., de Sterke, C. M., Krug, P. A., & Sipe, J. E. (1996). Bragg grating solitons. *Physical Review Letters, 76*, 1627.
2. Zayed, E. M., Alngar, M. E., Shohib, R. M., Biswas, A., Yıldırım, Y., Moraru, L., & Iticescu, C. (2022). Highly dispersive optical solitons in fiber Bragg gratings with quadratic-cubic nonlinearity. *Electronics, 12*, 125.
3. Zayed, E. M., Alngar, M. E., Shohib, R. M., Biswas, A., Yıldırım, Y., Khan, S., & Iticescu, C. (2022). Highly dispersive optical solitons in fiber Bragg gratings with Kerr law of nonlinear refractive index. *Mathematics, 10*, 2968.
4. Al-Ghafri, K. S., Sankar, M., Krishnan, E. V., Khan, S., & Biswas, A. (2023). Chirped gap solitons in fiber Bragg gratings with polynomial law of nonlinear refractive index. *Journal of the European Optical Society-Rapid Publications, 19*, 30.
5. Ghayad, M. S., Badra, N. M., Ahmed, H. M., Rabie, W. B., Mirzazadeh, M., & Hashemi, M. S. (2024). Highly dispersive optical solitons in fiber Bragg gratings with cubic-quadratic nonlinearity using improved modified extended tanh-function method. *Optical and Quantum Electronics, 56*, 1184.
6. Meng, L., Li, J., & Tao, J. (2015). Blow-up for the stochastic nonlinear Schrödinger equations with quadratic potential and additive noise. *Boundary Value Problems, 2015*, 132.
7. Zayed, E. M., Arnous, A. H., Seçer, A., Ozisik, M., Bayram, M., Shah, N. A., & Chung, J. D. (2023). Highly dispersive optical solitons in fiber Bragg gratings for stochastic Lakshmanan-Porsezian-Daniel equation with spatio-temporal dispersion and multiplicative white noise. *Results in Physics, 55*, 107177.
8. Zayed, E. M., Alngar, M. E., Shohib, R. M., Biswas, A., Yıldırım, Y., Moraru, L., & Georgescu, P. L. (2023). Dispersive optical solitons with differential group delay having multiplicative white noise by Itô calculus. *Electronics, 12*, 634.
9. Lashkin, V. M. (2024). Dynamics of multidimensional fundamental and vortex solitons in random media. *Physical Review E, 109*, 064216.
10. Zayed, E. M., Gepreel, K. A., & El-Horbaty, M. (2023). Highly dispersive optical solitons in fiber Bragg gratings with stochastic perturbed Fokas-Lenells model. *Optik, 286*, 170975.
11. Tang, L. (2025). Qualitative analysis, chaotic behavior and optical solitons perturbation for the coupled Fokas-Lenells system in birefringent fibers. *Qualitative Theory of Dynamical Systems, 24*, 59.
12. Jahan, M., Ullah, M., Rahman, Z., & Akter, R. (2025). Novel dynamics of the Fokas-Lenells model in birefringent fibers applying different integration algorithms. *International Journal of Mathematical and Computational Engineering, 3*, 1–12.
13. Zayed, E. M., El-Horbaty, M., Alngar, M. E., & El-Shater, M. (2022). Dispersive optical solitons for stochastic Fokas-Lenells equation with multiplicative white noise. *Eng, 3*, 523–540.
14. Lashkin, V. M. (2021). Perturbation theory for solitons of the Fokas-Lenells equation: Inverse scattering transform approach. *Physical Review E, 103*, 042203.
15. Ai, L., & Xu, J. (2019). On a Riemann-Hilbert problem for the Fokas-Lenells equation. *Applied Mathematics Letters, 87*, 57–63.
16. Cheng, Q., & Fan, E. (2023). The Fokas-Lenells equation on the line: Global well-posedness with solitons. *Journal of Differential Equations, 366*, 320–344.
17. Zhang, Y., Qiu, D., & He, J. (2023). Explicit nth-order solutions of Fokas-Lenells equation based on revised Riemann-Hilbert approach. *Journal of Mathematical Physics, 64*.
18. He, J., Xu, S., & Porsezian, K. (2012). Rogue waves of the Fokas-Lenells equation. *Journal of the Physical Society of Japan, 81*, 124007.
19. Zhao, Y., & Fan, E. (2021). Inverse scattering transformation for the Fokas-Lenells equation with nonzero boundary conditions. *Journal of Nonlinear Mathematical Physics, 28*, 38–52.
20. Ullah, M. S., Roshid, H. O., & Ali, M. Z. (2023). New wave behaviors of the Fokas-Lenells model using three integration techniques. *PLoS ONE, 18*, e0291071.
21. Li, Z. L. (2010). Periodic wave solutions of a generalized KdV-mKdV equation with higher-order nonlinear terms. *Zeitschrift für Naturforschung A, 65*, 649–657.
22. Metwally, A. S., Alngar, M. E., Shohib, R. M., Shah, S. A., & Biswas, A. (2026). Highly dispersive optical solitons with differential group delay and multiplicative white noise having Kerr law of self-phase modulation. *Ukrainian Journal of Physical Optics, 27*(3), 03196–03224.
23. Li, S., Qian, S., Chen, H., Song, J., & Cao, A. (2021). An extended nonlinear Schrödinger equation for water waves with linear shear flow, wind, and dissipation. *AIP Advances, 11*.
24. Zabolotnykh, A. A. (2023). Nonlinear Schrödinger equation for a two-dimensional plasma: Solitons, breathers, and plane wave stability. *Physical Review B, 108*, 115424.
25. Kengne, E., Liu, W. M., & Malomed, B. A. (2021). Spatiotemporal engineering of matter-wave solitons in Bose-Einstein condensates. *Physics Reports, 899*, 1–62.
26. Hasan, W. M., Ahmed, H. M., Ahmed, A. M., Rezk, H. M., & Rabie, W. B. (2025). Exploring highly dispersive optical solitons and modulation instability in nonlinear Schrödinger equations with nonlocal self-phase modulation and polarization dispersion. *Scientific Reports, 15*, 27070.

27. Kolkowski, R., Hakala, T. K., Shevchenko, A., & Huttunen, M. J. (2023). Nonlinear nonlocal metasurfaces. *Applied Physics Letters, 122*.
28. Sharma, M., Tal, M., McDonnell, C., & Ellenbogen, T. (2023). Electrically and all-optically switchable nonlocal nonlinear metasurfaces. *Science Advances, 9*, eadh2353.
29. Jiang, H., Cai, Y., & Han, Z. (2024). Enhanced high-harmonic generation with spectral tunability in nonlocal metasurfaces enabled by quasiguided modes. *Physical Review B, 110*, 245424.
30. Zhang, D. (2023). Stochastic nonlinear Schrödinger equations in the defocusing mass and energy critical cases. *Annals of Applied Probability, 33*, 3652–3705.
31. Khan, A., Muhammad, J., Younas, U., Thinakaran, R., Abdeljawad, T., & Alqudah, M. A. (2025). Investigating the stochastic higher dimensional nonlinear Schrödinger equation for telecommunication engineering. *Scientific Reports, 15*, 27309.
32. Cui, J., Liu, S., & Zhou, H. (2023). Optimal control for stochastic nonlinear Schrödinger equation on graph. *SIAM Journal on Control and Optimization, 61*, 2021–2042.
33. Kaur, L., Arnous, A. H., Murad, M. A. S., & Biswas, A. (2026). Dispersive optical soliton perturbation with Schrödinger-Hirota equation by Lie symmetry. *Ukrainian Journal of Physical Optics, 27*(3), 03239.
34. Arnous, A. H., Murad, M. A. S., Yıldırım, Y., & Biswas, A. (2026). Quiescent vector optical solitons with nonlinear dispersion. *Ukrainian Journal of Physical Optics, 27*(4), 04054–04076.
35. Zayed, E. M., Ahmed, M. S., Arnous, A. H., & Yıldırım, Y. (2025). Novel soliton solutions of the (3+1)-dimensional stochastic nonlinear Schrödinger equation in birefringent fibers. *Chaos, Solitons & Fractals, 194*, 116152.

Metwally, A.S.M., Alngar, M.E.M., Shohib, R.M.A., Shirsath, S.E., Biswas A. (2026). Stochastic (3+1)-Dimensional Spatio-Temporal Solitons in a Generalized Effective Fiber Bragg-Grating Envelope Model. Ukrainian Journal of Physical Optics, 27(4), 04102 – 04127.
doi: 0.3116/16091833/Ukr.J.Phys.Opt.2026.04102

Анотація. *У цій статті досліджується нова (3+1)-вимірна зв'язана нелінійна система рівнянь Шредінґера (NLS), яка враховує стохастичні ефекти білого шуму у волоконних брегівських ґратках (FBG). Модель описує взаємодію двох ортогонально поляризованих комплексних функцій обвідної, які зазнають впливу хроматичної та просторово-часової дисперсії, само- та крос-фазової модуляції, інтермодового зв'язку та випадкових флуктуацій. Застосовуючи модифікований метод Sub-ODE, отримано широкий клас точних аналітичних розв'язків, зокрема яскраві та темні солітони, сингулярні розв'язки й періодичні хвильові розв'язки. Також отримано явні розв'язки, виражені через еліптичні функції Якобі та Веєрштраса, що забезпечує єдиний опис нелінійних хвильових структур, зумовлених стохастичними ефектами. Фізично результати демонструють, як інтенсивність шуму впливає на амплітуду солітона, його локалізацію та фазову модуляцію, тим самим пов'язуючи детерміновані та стохастичні режими. Теоретичні результати мають значення для систем оптичного зв'язку, конденсатів Бозе–Ейнштейна, плазмових середовищ, а також нелінійних біологічних і хімічних систем, у яких випадкові флуктуації відіграють важливу роль.*

Ключові слова: *стохастичне нелінійне рівняння Шредінгера, волоконні брегівські ґратки, яскраві та темні солітони, розв'язки еліптичних функцій, динаміка, керована шумом*